JCI The Journal of Clinical Investigation

Loss of the sphingolipid desaturase DEGS1 causes hypomyelinating leukodystrophy

Devesh C. Pant, … , Odile Boespflug-Tanguy, Aurora Pujol

J Clin Invest. 2019. https://doi.org/10.1172/JCI123959.

Research | In-Press Preview | Neuroscience

Graphical abstract

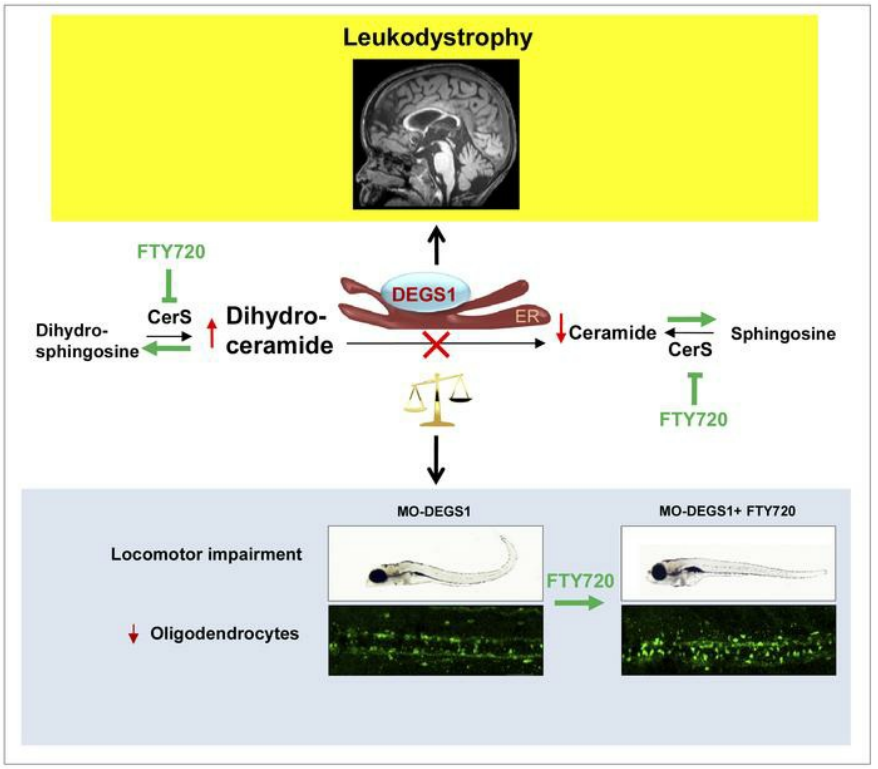

Find the latest version:

http://jci.me/123959/pdf

Loss of the sphingolipid desaturase DEGS1 causes hypomyelinating leukodystrophy

Devesh C Pant PhD[1,2], Imen Dorboz PhD[3], Agatha Schluter PhD[1,2], Stéphane Fourcade PhD[1,2], Nathalie Launay PhD[1,2], Javier Joya PhD[1,2], Sergio Aguilera-Albesa MD[4], Maria Eugenia Yoldi MD[4] Carlos Casasnovas MD[1,2], Mary J. Willis MD[5], Montserrat Ruiz PhD[1,2], Dorothée Ville MD[6], Gaetan Lesca MD[7], Karine Siquier-Pernet PhD[8,9], Isabelle Desguerre MD[8,9], Huifang Yan PhD[10,11], Jinming Wang PhD[10,11], Margit Burmeister PhD[10,11], Lauren Brady PhD[12], Mark Tarnopolsky MD[13], Carles Cornet MSc[14], Davide Rubbini PhD[14], Javier Terriente PhD[14], Kiely N. James MSc[15], Damir Musaev PhD[15], Maha S. Zaki MD[16], Marc C Patterson MD[17], Brendan C Lanpher MD[18], Eric W Klee PhD[18,19], Filippo Pinto e Vairo MD[18,19], Elizabeth Wohler MS[20], Nara Lygia de M. Sobreira MD[21], Julie S. Cohen MSc[22], Reza Maroofian PhD[23], Hamid Galehdari PhD[24], Neda Mazaheri MSc[24,25], Gholamreza Shariati MD[25,26], Laurence Colleaux PhD [8,9], Diana Rodriguez MD[27,28], Joseph G. Gleeson MD[15], Cristina Pujades PhD[29], Ali Fatemi MD[22,30], Odile Boespflug-Tanguy MD[31*]and Aurora Pujol MD[1,2,32*]

[1]Neurometabolic Diseases Laboratory, Bellvitge Biomedical Research Institute (IDIBELL), 08908 L'Hospitalet de Llobregat, Barcelona, Catalonia, Spain
[2]Center for Biomedical Research on Rare Diseases (CIBERER), ISCIII, Madrid, Spain
[3]INSERM UMR 1141, DHU PROTECT, Paris Diderot University, Sorbonne Paris Cité, France, Paris 06, Paris, France.
[4]Pediatric Neurology Unit, Department of Pediatrics, Navarra Health Service, Navarrabiomed, Pamplona, Spain.
[5]Department of Pediatrics, Naval Medical Center San Diego, San Diego, CA, USA
[6]Department of Neuropediatrics, Lyon University Hospital, Lyon, France
[7]Department of Medical Genetics, Lyon University Hospital and GENDEV team CNRS UMR 5292, INSERM U1028, CRNL, and University Claude Bernard Lyon 1, Lyon, France
[8]Paris Descartes - Sorbonne Paris Cité University, Imagine Institute, Paris, France
[9]Laboratory of developmental brain disorders, INSERM UMR 1163, Paris, France
[10]Department of Psychiatry, University of Michigan, Ann Arbor, MI, USA.
[11]Department of Human Genetics, University of Michigan, Ann Arbor, MI, USA
[12]Department of Pediatrics (Neuromuscular and Neurometabolics), McMaster Children's Hospital, Hamilton, Ontario, Canada.
[13]Departments of Pediatrics (Neuromuscular and Neurometabolics), and Medicine, McMaster University, Hamilton, Ontario, Canada.
[14]ZeClinics SL, PRBB, Barcelona, Spain
[15]Laboratory for Pediatric Brain Disease, Department of Neurosciences, Howard Hughes Medical Institute, University of California, San Diego, CA, USA.
[16]Human Genetics and Genome Research Division, Clinical Genetics Department, National Research Centre, Cairo, Egypt.
[17]Departments of Neurology and Pediatrics, Mayo Clinic, Rochester, MN, USA.
[18] Department of Clinical Genomics, Mayo Clinic, Rochester, MN, USA
[19]Center for Individualized Medicine, Department of Health Sciences Research, Mayo Clinic, Rochester, MN, USA
[20]McKusick-Nathans Institute of Genetic Medicine, Johns Hopkins University School of Medicine, Baltimore, MD, USA.

[21]McKusick-Nathans Institute of Genetic Medicine, and Department of Pediatrics, Johns Hopkins University School of Medicine, Baltimore, MD, USA.
[22]Moser Center for Leukodystrophies at Kennedy Krieger Institute, 707 North Broadway, Baltimore, MD, 21205, USA.
[23]Genetics Research Centre, Molecular and Clinical Sciences Institute, St George's, University of London, London, UK
[24]Department of Genetics, Faculty of Science, Shahid Chamran University of Ahvaz, Ahvaz, Iran
[25]Narges Medical Genetics and Prenatal Diagnosis Laboratory, East Mihan Ave., Kianpars, Ahvaz, Iran
[26]Department of Medical Genetics, Faculty of Medicine, Ahvaz Jundishapur University of Medical Sciences, Ahvaz, Iran
[27]APHP, Department of Neuropediatrics, National Reference Center for Neurogenetic Disorders, Hôpital Armand-Trousseau, GHUEP, Paris, France.
[28]GRC ConCer-LD, Sorbonne Universités, UPMC Université, Paris, France
[29]Department of Experimental and Health Sciences, Universitat Pompeu Fabra, Barcelona, Spain
[30]Department of Neurology, Johns Hopkins Medical Institutions, Baltimore, MD, USA
[31]Assistance Publique des Hopitaux de Paris (APHP), Reference Center for "Leukodystrophies and rare leukoencephalopathies," (LEUKOFRANCE), Hôpital Robert Debré, Paris, France.
[32]Catalan Institution of Research and Advanced Studies (ICREA), Barcelona, Catalonia, Spain

[*]Correspondence should be addressed to:
*Professor Aurora Pujol, Neurometabolic Diseases Laboratory, IDIBELL, Hospital Duran i Reynals, Gran Via 199, 08908 L'Hospitalet de Llobregat, Barcelona, Spain. Tel: +34 932607137; Fax: +34 932607414; Email: apujol@idibell.cat

*Professor Odile Boespflug-Tanguy, INSERM UMR 1141, DHU PROTECT, Paris Diderot University, Sorbonne Paris Cité, France
Email : odile.boespflug-tanguy@aphp.fr

ABSTRACT

Sphingolipid imbalance is the culprit in a variety of neurological diseases, some affecting the myelin sheath. We have used whole exome sequencing in patients with undetermined leukoencephalopathies to uncover the endoplasmic reticulum lipid desaturase *DEGS1* as the causative gene in nineteen patients from thirteen unrelated families. Shared features among the cases include severe motor arrest, early nystagmus, dystonia, spasticity and profound failure to thrive. MRI showed hypomyelination, thinning of corpus callosum and progressive thalami and cerebellar atrophy, suggesting a critical role of DEGS1 in myelin development and maintenance. This enzyme converts dihydroceramide (DhCer) into ceramide (Cer) in the final step of the *de novo* biosynthesis pathway. We detected a marked increase of the substrate DhCer and DhCer/Cer ratios in patient's fibroblasts and muscle. Further, we used a knockdown approach for disease modelling in *Danio rerio,* followed by a preclinical test with the first-line treatment for multiple sclerosis, fingolimod (FTY720, Gilenya®). The enzymatic inhibition of ceramide synthase, one step prior to DEGS1 in the pathway, by fingolimod, reduced the critical DhCer/Cer imbalance and the severe locomotor disability, increasing the number of myelinating oligodendrocytes in the zebrafish model. These proof-of-concept results pave the way to clinical translation.

Keywords

DEGS1; Hypomyelinating Leukodystrophy; Sphingolipids; Ceramides; Fingolimod

Introduction

Leukodystrophies (LD) are a heterogeneous group of rare, heritable disorders of all ages that primarily affect the brain's white matter, often leading to motor and cognitive impairment in early childhood and progression to severe disability over time (1, 2). All modes of inheritance, broad pathogenic mechanisms, and complex cellular interactions underlie LD, yet many cases remain unexplained with an unknown biochemical or molecular basis (3). With progress in clinical genomics, new forms of ultra-rare leukodystrophies are being recognized (4-6), and advances in novel technologies in gene, cell and enzyme therapy hold promise for improving patient management (7, 8).

Using whole exome sequencing (WES), we have identified homozygous or compound heterozygous pathogenic variants in the *DEGS1* gene in nineteen leukodystrophy patients from thirteen unrelated families. *DEGS1* was first cloned in 1996 from *Drosophila melanogaster*, and was given the name ''drosophila degenerative spermatocyte 1" or *DEGS1* (9). It encodes a Δ4-dihydroceramide desaturase (OMIM 615843) mapping to chromosome 1q42.11, also known as *DES1*. This enzyme catalyzes the insertion of a Δ 4,5-trans double bond into dihydroceramide (DhCer) to convert it to ceramide (Cer), in the final step of the *de novo* ceramide biosynthesis pathway (Figure 1) (10).

Biosynthesis of Cer, made of a sphingoid base and a fatty acid, mainly occurs via three distinct pathways: a) the *de novo* pathway, which takes place in the endoplasmic reticulum (ER) and uses palmitoyl-CoA and serine as its precursors; b) the sphingomyelinase pathway, which takes place in the plasma membrane, Golgi apparatus and mitochondria, and converts sphingomyelin into Cer bi-directionally; and c) the salvage pathway, which converts complex sphingolipids species into Cer and recycles the acyl moiety of ceramides in both lysosomes and endosomes (Figure 1) (11). This compartimentalization of the more than 200 structurally distinct ceramides suggests a high complexity of regulation and function, which is only beginning to emerge (12, 13).

Cer is the central unit of all sphingolipids, serving as a building block and as a hub for bioactive, more complex lipidic species. The biosynthesis of Cer is followed by the addition of sugar moieties to generate glucosylceramide and galactosylceramide, which undergo further transformation into gangliosides and sulfatides, respectively. Galactosylceramides and sulfatides with very long N-acyl chains, in particular C24:0 and C24:1, are the most abundant myelin lipid components (14, 15). Indeed, defects of

galactosylceramidase and arylsulfatase A, one and two steps after DEGS1 respectively, cause Krabbe disease/globoid leukodystrophy (GLD) and metachromatic leukodystrophy (MLD) (Figure 1), two well-characterized demyelinating LD. Beyond the myelin sheath, sphingolipids are involved in numerous biological processes related to cell survival, metabolic regulation and adaptation to stressors (16). The importance of sphingolipids in neurodegenerative disease has recently expanded beyond lysosomal disorders or classical sphingolipidosis. Secondary disturbances of these lipid species including DhCer have been shown in Huntington disease (17) and Alzheimer's patients (18).

Evidence from studies in animal models supports an essential role of *DEGS1* in development (19, 20). Homozygous *Degs1*$^{-/-}$ mice die within the first 8 weeks of age, presenting a complex phenotype, including small size, scaly skin, sparse hair and tremors (19). Lipidomics analysis showed that *Degs1*$^{-/-}$ mice exhibit accumulation of DhCer and higher DhCer/Cer ratio in several tissues (19), similarly to the *Drosophila melanogaster* model (20).

Our patients presented with hypomyelinating LD with progressive atrophy of corpus callosum (CC), thalami and cerebellum, severe failure to thrive and peripheral neuropathy. Using patients' fibroblasts, we functionally validated variants by testing their impact on DhCer/Cer ratios and reactive oxygen species (ROS) production. Importantly, treatment with fingolimod (FTY720), a drug targeting sphingolipid metabolism and broadly used treatment for relapsing-remitting multiple sclerosis (MS), improved the metabolic imbalance, numbers of myelin-producing oligodendrocytes and locomotor deficits in the zebrafish model.

Results

Bi-allelic deleterious variants of *DEGS1* in patients with brain white matter abnormalities

As part of our ongoing studies on the molecular basis underlying undiagnosed leukoencephalopathies, we identified a total of 19 individuals from 13 unrelated families with rare variants suspected to alter DEGS1 function (Figure 2; Table 1-2). The first patient under investigation was a female who presented feeding difficulties since birth, extreme irritability, hypertonia with opisthotonus, and nystagmus, resulting in death at 18 months. Severe hypomyelination was observed in the central and peripheral nervous system in the MRI and nerve conduction studies (Individual 6, Table 1-3). Extensive diagnostic investigations were negative. We thus carried out WES (see Experimental Procedures) in the proband, with subsequent Sanger validation and segregation analysis (Supplementary Figure 1). We identified an homozygous frameshift variant in *DEGS1* (GenBank ID: NM_003676.3, c.604delT; p.(Tyr202Thrfs*8)) that was not present in the genome aggregation database (GnomAD; >246,000 chromosomes), the NHLBI Exome Variant Server (EVS; >13,000 alleles), or the Exome Aggregation Consortium (ExAC) database (ExAC> 60.706 individuals). No homozygous loss-of-function (LoF) variants were present for this gene in the mentioned databases. Personal communication with international Reference Centers for Leukodystrophies and information exchange on the GeneMatcher (21) platform facilitated the identification of 18 additional affected individuals with *DEGS1* variants from various ethnical backgrounds who displayed overlapping phenotypes. These variants were present in a homozygous or compound heterozygous manner in thirteen families and segregated in the recessive inheritance mode. Consanguinity was present in 2/3 of the families. All consanguineous families harbor a homozygous variant except family 9.

DEGS1 encodes an evolutionary conserved sphingolipid desaturase of 323 AA containing six transmembrane domains, three histidine motifs, a lipid desaturase domain and a fatty acid desaturase (FAD) domain (Figure 2). The highly-conserved histidine motifs $HX_{(3–4)}H$, $HX_{(2–3)}HH$, and $H/QX_{(2–3)}HH$, are essential for catalytic activity (10). Twelve out of thirteen variants are located in the FAD domain, and only one, p.(Met37Thr), is located in the sphingolipid delta4-desaturase domain. The most prevalent *DEGS1* variants in our cohort were p.(Asn255Ser) and p.(Trp107*), identified

in three and two independent families, respectively. Eight out of thirteen variants have not been identified in control populations, and the rest of the variants have a MAF lower than 0.0001, with none being found in the homozygous state in the ExAC, GnomAD, 1000 Genomes, Iranome or GME Variome databases. Seven out of thirteen variants are nonsense with four stopgain and three frameshifts. Six out of thirteen variants are missenses with high deleteriousness predicted by most of the 15 *in silico* tools tested (Supplementary Table S1).

Clinical features

Among the 19 affected patients, age of onset was at 5.6 months (+/- 7.2 m; 0.5-24 months) with variable disease severity. Fifteen of the patients (79 %) presented a severe form characterized by a very poor psychomotor development, dystonia and severe spasticity (Table 1-2 and Supplementary Video). All except one subject presented early nystagmus or abnormal eye movements between 1 and 6 months of age. Seizures were frequently observed (80%) around 2 years of age with a pharmaco-resistant epilepsy sensitive to ketogenic diet in only 3 cases. In this group, failure to thrive was the most worrying clinical issue after 2 years of age despite feeding through gastrostomia. Head circumference was relatively conserved with acquired microcephaly (< 2 DS) in only 3 cases. Death occurred in 4 patients (26%) at a mean age of 4.6 years (+/-1.9; 2.5-7 y). These 4 patients harbored LoF variants (Table 1-2).

In the remaining 22% of the patients) (patients 3, 7, 8, 14), a less severe phenotype was observed. Acquisition was better with capacity to sit or walking and to use a verbal communication. Progressive spasticity developed rapidly in these patients leading to motor degradation at various ages (2 to 16y). None presented with growth impairment (<2SD) or microcephaly (Table 1-2).

Cerebral MRI images were available for review by expert clinicians (AF, SAA, CC, DR, OBT) for 18 patients at mean age 3.6 y (+/-4.2; 0.5-17 y) (Table 3). All patients showed T2/FLAIR hyperintense white matter lesions with a normal hyperintense T1 indicative of an hypomyelinating form of LD (Figure 3 and Supplementary Figure 2) (22). In the 3 mildest clinical forms of the disease (patients 7, 8, 14), the abnormal WM signal affected the deep white matter with a relative preservation of the subcortical regions (Figure 3A, patient 7). In two severe cases a demyelinating aspect of the posterior subcortical-deep WM was noticed on T1 (Supplementary Figure 2, patients 4 and 10). Despite the severity of the clinical

symptoms, myelination progressed in the 6 patients analyzed with 2 or more MRI and a mean follow up of 4.2 y (+/-3.5 y; 1-10 y) (Figure 3B and Supplementary Figure 2).

Basal ganglia abnormalities were observed in only the most severe forms. Abnormal hyper T2/FLAIR signal and atrophy of the thalami were the most frequent findings (11/15 cases, 73%) (Figure 3, Table 3, Supplementary Figure 2). Two severe patients (patient 2 and 19) showed an associated hypoT2/FLAIR in the *pallidi* (Table 3).

Thinning of the CC was observed in 76 % of cases associated with progressive vermian cerebellar atrophy in 41% of cases (Figure 3, Supplementary Figure 2). Demyelinating neuropathy with nerve conduction below 35m/s was observed in 5 out of the 14 patients analyzed by EMG /NCV (1/3). The evoked potentials performed in 7 patients (4 BAEP; 5 VEP; 1 SEP) demonstrated long latencies in the central conduction (> 3 SD) in all cases (Table 1-2).

Genotype-phenotype correlation

Patients from the same families (Table 1-2, see families 1, 3, 5, 8, 10) as well as patients with the same genotype (Table 1-2, see Algerian families 6 and 7; Egyptian families 8 and 12), expressed the same phenotype. Patients 2, 6, 11 and 12 who harbored homozygous LoF variants in the FAD domain, died at 7 years, 18 months, 2.5 and 5 years of age respectively, indicating a likely phenotype-genotype correlation. At the other end of the spectrum we found patient 3, a 9-year-old girl with p.(Arg133Trp) and p.(Leu251Phefs*10) variants *in trans*, who presented with developmental regression from 9 months of age; however she was able to sit without help and communicate using simple sentences. Her MRI and spectroscopy were almost normal at 4 and 5 years of age and presented no signs of peripheral neuropathy.

DEGS1 activity is impaired in patients' fibroblasts and muscle

To verify the impact of the variants on DEGS1 protein function, we used targeted lipidomics to quantify dihydroceramides and ceramides, the substrates and products of DEGS1 respectively. The results indicate a slight reduction of ceramides (Cer) concomitant with an important accumulation (3 to 9 fold) of dihydroceramides (DhCer) in cultured skin fibroblasts of affected individuals (patients 4, 7, 9) and muscle tissue (patient 3). Thus, the activity of the DEGS1 enzyme, represented as the DhCer/Cer ratio, was greatly decreased in all cases (Figure 4A-B), consistent with the notion that the variants identified caused reduced activity of the DEGS1 enzyme.

Impaired function of DEGS1 induces intracellular ROS production

Excess of dihydroceramides has been recently reported to generate ROS in *Drosophila ifc* KO photoreceptors (20). We observed that ROS production was increased in all patients' fibroblasts (patients 4, 7 and 9) compared to controls (Figure 4C), using the probe H_2DCFDA which measures singlet oxygen, superoxide, hydroxyl radical and various peroxides and hydroperoxides (23). To gain insight into the direct consequences of DhCer accumulation in our system, we incubated control and patients fibroblasts with a long-chain DhCer (C18:0-DhCer) for 6h, at a dose of 20 µM. This dose increased ROS production in control fibroblasts although we could not discern an increase in the patient fibroblasts (Figure 4D). At higher doses, we found toxic effects in the fibroblasts independent of phenotype. This result confirmed that DhCer excess can generate ROS in human fibroblasts, whereas the blunted response in patient fibroblasts may follow saturation effects due to the steady-state accumulation of DhCer.

***Degs1* is highly expressed in the central nervous system (CNS)**

We performed RT-qPCR expression studies in different child and adult control human CNS tissues (n=2), to find specific expression of this gene in frontal lobe BA9, putamen, entorhinal cortex, hippocampus, hypothalamus, pons, cerebellum, white matter frontal cortex, spinal cord (Supplementary Figure 3A). This is consistent with the expression of *Degs1* mRNA in different tissues of 4 month old wild type mice (n=3), with high expression in the CNS, in particular in spinal cord, brain cortex, pons, cerebellum and hippocampus, compared to other organs (Supplementary Figure 3B). We next performed RT-qPCR to assess the *DEGS1* mRNA expression in fibroblasts from affected individuals (patients 4, 7 and 9) and healthy age-matched control individuals. We observed a 50% decrease in patient 4 (Supplementary Figure 3C), possibly owing to mRNA decay in the allele bearing the stop variant. We also analyzed the expression of *DEGS2*, the closest paralog of *DEGS1*, which is reported to have a partially overlapping, low C4-desaturase activity while showing a high C4-hydroxylase activities (24, 25). We corroborated a high expression of DEGS2 in small intestine and kidney (24), comparable to *DEGS1* (Supplementary Figure 3B), and two orders of magnitude lower expression in mouse brain and human fibroblasts as compared to *DEGS1*, which argues against any putative, physiologically relevant compensatory role of *DEGS2* (Supplementary Figure 3B-C).

Loss of *Degs1* in zebrafish causes DhCer/Cer imbalance, reduced number of oligodendrocytes and locomotor impairment

We investigated the suitability of a zebrafish model for this disease, since many of the genetic pathways for myelin development and maintenance are conserved (26). There is a single zebrafish ortholog of human DEGS1 (NP_997865.1), sharing a 74% protein identity with human DEGS1 (NP_003667.1). *In situ* hybridization (ISH) studies showed that *Degs1* was expressed in the dorsal part of the zebrafish brain, being more prominent in the dorsal thalamus, the posterior tuberculum, the tectum opticum, the hindbrain and the spinal cord (Supplementary Figure 4A-B). Using a transgenic strain expressing EGFP under the control of the myelin basic protein (mbp) promoter labeling myelinating oligodendrocytes (MBP^+) (27), we found overlapping pattern of *Degs1* to MBP^+ cells (Supplementary Figure 4C-F). Thus, we knocked down *Degs1* in zebrafish, by designing an efficient splice-blocking morpholino (MO) (Supplementary Figure 4G-I). Downregulation of DEGS1 induced an increase of DhCer and of the DhCer/ Cer ratio (Figure 5A) at 5 days post-fertilization (5 dpf). Moreover, a high percentage of MO-DEGS1 larvae displayed an abnormal morphology (Figure 5B-C).

Next, phenotype and swimming ability of MO-DEGS1 zebrafish larvae was analyzed by measuring the total movement distance and by comparing the activity displayed by uninjected, and MO-control injected larvae. The total movement distance (mm) in MO- DEGS1 larvae was very significantly reduced (Figure 5D-E). Importantly, when embryos were injected with 10 ng of MO-DEGS1, no significant differences were observed in the survival rate compared to embryos injected with MO-controls or uninjected animals. To test the effect on myelination of the knockdown of DEGS1 in zebrafish, we measured the number of MBP^+ cells in the spinal cord at 4·5 dpf after MO-DEGS1 injection (27). Interestingly, we found that the number of MBP^+ cells was reduced by 30 % in MO-DEGS1 compared to control larvae (Figure 5F-G'). Altogether, these results indicate that loss of DEGS1 function in zebrafish larvae results in some ten- fold increased DhCer/Cer ratio, locomotor disability and impaired myelination, consistent with the patients' phenotype.

FTY720 ameliorates in the phenotype of MO-DEGS1 zebrafish, while reducing ROS levels in patient fibroblasts

Drug screening in zebrafish has been successfully used to identify target pathways as well as therapeutic compounds for human diseases (28). In an attempt to provide a therapeutic option for this life-threatening condition, we chose an FDA-approved drug targeting the *de novo* ceramide biosynthesis pathway, fingolimod (FTY720). This pleiotropic drug is reported to act as an inhibitor of the enzyme prior to DEGS1, the ceramide synthase (CerS) (Figure 1) (29). We used concentrations of 3·3, 1·0 and 0·3 ng/µl of FTY720, from birth to 120 hpf, without observing deleterious effects on survival. Also the number of MBP^+ signals along the spinal cord was raised in MO-DEGS1 larvae after treatment, approaching the number of MBP^+ cells in control larvae (Figure 5F-J). The locomotor deficit of MO-DEGS1 larvae was remarkably ameliorated after 5 days of treatment with FTY720 at 1·0 ng/µl (Figure 6A-B). This recovery correlated with an amelioration of total DhCer levels and ratios of DhCer/Cer upon treatment (Figure 6C). The effect of the drug was more marked towards some DhCer species (the saturated and monounsaturated C16- ,C17-, C18-, C20-, C22-, C24-, C26-, C28-DhCer), which also accumulated the most. Of note, a ten fold decrease of C10-Cer was also observed, and recovered with treatment (Supplemental Table S2). Next, we tested a potential protective effect of FTY720 on ROS generation in DEGS1-fibroblasts (patients 4, 7 and 9 as above), by using a dose of 5 µM for 6 h and measuring the ROS levels as described above. FTY720 treatment prevented the elevation of ROS levels in patient fibroblasts (Figure 6D), while no effect was seen in control fibroblasts. These results provide proof of principle that FTY720 reduces the accumulation of DhCer and, thus, results in diminished ROS production at the cellular level.

Discussion

This study highlights the interest of using freely accessible information exchange platforms such as GeneMatcher after exome sequencing, for rapid identification of molecular causes of ultrarare disorders and collection of sufficient cases to delineate a disease spectrum and improve management (30).

Patients with DEGS1-related LD shared clinical and MRI features of hypomyelinating LD. In this heterogeneous group of LD, a large clinical spectrum of disease severity has been described in terms of defective myelination and axonal suffering. A large majority of our DEGS1 patients present the severe form of hypomyelinating LD, accompanied by thin CC and cerebellar atrophy as observed with TUBB4-related LD (31). However, the hypomyelination observed in TUBB4, as well as in the severe forms of PLP1-related LD, is more diffuse and remains stable over time (32). The relative preservation of the subcortical white matter relative to the clinical severity of DEGS1-patients may represent an interesting MRI diagnostic feature. Likewise, the observed improvement in myelination in our patients contrasts with the progressive atrophy affecting first the CC, then thalami and cerebellum, and finally the whole brain. This suggests a critical role of DEGS1 and ceramide metabolism in myelin development and maintenance, but also in neuronal/ axonal functioning. The hypomyelinating pattern of the deep WM and the T2 hyperintensities of the thalamic regions are also observed in infantile GM1/GM2 gangliosidosis (22, 33). Finally, the association of central and peripheral demyelination are the hallmarks of disorders of sphingolipid metabolism (MLD and GLD), and of the peroxisomes (34). Although individual features in the DEGS1-related patients are not specific, their combination results in a defined pattern distinguishable from other LD.

The importance of maintaining sphingolipid balance for the nervous system is well exemplified in the lysosomal disorders such as Gaucher, Niemann Pick or Farber, all one enzymatic step away from DEGS1 (Figure 1) (8). Indeed, in many lipid storage disorders, deficiency or malfunctioning of one of the enzymes involved in sphingolipid metabolism results in accumulation of the corresponding lipid substrate leading to cellular dysfunction and death. Accumulation of DhCer is involved in many stress signals such as cell cycle regulation, autophagy induction, apoptosis and ROS generation (35, 36); the latter being substantiated by our results. Redox imbalance is intertwined with energy homeostasis in diseases of myelin (23, 37), and may play a role in the cachexia observed, in the large majority of our patients. Moreover, suppressing

DEGS1 led to cell cycle arrest, cell growth inhibition and apoptosis in cell culture models (16, 38), which may explain the decrease of myelinating MBP+ oligodendrocyte numbers and perhaps contribute to the general developmental delay and impressive failure to thrive in our patients. Concerning the biogenesis and stability of the myelin sheath, an enhanced proportion of DhCer (in particular C16-DhCer) has recently been shown to destabilize model membranes by increasing permeability and the formation of rigid domains (35). Of note, C16-DhCer is increased in our MO-DEGS1 model and lowered by fingolimod treatment (Supplementary Table S2). It is therefore tempting to posit that the exquisitely regulated process of myelin sheath biogenesis and compaction, including the lipid-lipid and lipid-protein interactions with major protein players such as MBP, MAG or PLP (14, 39), is likely to be severely disturbed, simply by the biophysical consequences of the DhCer/Cer imbalance on the cellular membranes.

Further, it has been recently shown that in the Drosophila (*ifc*) KO, photoreceptor degeneration was caused by increased DhCer, not reduced levels of Cer (20). Along the same lines, Cer reduction by itself appears to have a positive effect by enhancing myelin repair in acute and chronic demyelination paradigms, as deduced from a model of acid sphingomyelinase deficiency (40). Of note, impairment of the alkaline ceramidase 3 (ACER3), just one step after DEGS1 (Figure 1), causes a recently described form of childhood leukoencephalopathy of similar clinical presentation to the DEGS1-related LD, with an hypomyelinating aspect of the periventricular and deep WM, severe brain atrophy by 5 years of age, and peripheral neuropathy (5). It is intriguing that the plasma profile of the described patient showed mainly accumulation of DhCer, along with various Cer forms and lactosylceramides in lesser extent (5). Further investigations will be necessary to determine the precise molecular mechanisms through which excess of DhCer, may be toxic for myelinating oligodendrocytes or for the biogenesis of the myelin sheath. By the same token, and beyond the plausible direct negative effects of substrate accumulation in this case, we should acknowledge that sphingolipid metabolism constitutes an intricate network coupled in a "metabolic ripple" (16). As such, the loss of a given enzyme function may cause a shift in the substrate specificity of other enzymes in the pathway, leading to increased production of atypical lipid products that may be toxic to the cell (41). This intriguing possibility should be explored for DEGS1, likely by using a systems biology-type of approach, ideally including integration of comprehensive lipidomics and transcriptomics data (42). A bulk of evidence suggests that fingolimod has potential to become a lead player in

this context. Its success in relapsing-remitting MS relies on its activity as immunosuppressant, acting by sequestering circulating mature lymphocytes to the lymph nodes, and preventing their penetration into the brain and subsequent myelin destruction. Its molecular effects promoting neuron and oligodendrocytes survival are based on the structural similarity of FTY720 to sphingosine, which allows it to work as a *bona-fide* functional antagonist to S1P receptors (43, 44), and has lately shown to even improve microstructural integrity and myelination in the white matter tracts of human MS patients (45).

In part because of this structural similarity to sphingosine, FTY720 is a pleiotropic drug that also interferes with sphingolipid *de novo* biosynthesis, mainly by inhibiting ceramide synthase (CerS) (29, 43), the enzyme that converts sphinganine to DhCer, one step prior to DEGS1, and also converts sphingosine to ceramide (Figure 1). There are six CerS orthologs in mammals (46) and nine –due to whole genome duplication- in zebrafish (47). These enzymes transfer a variable length fatty acyl-coenzyme A (CoA) to the amine group of sphinganine or sphingosine. Studies employing genetic manipulations have demonstrated that different CerS isoforms exhibit strong preference for fatty acyl-CoAs with differing carbon chain lengths, although with extensive overlaps. CerS1 exclusively uses 18 carbon (C18) fatty acids, forming C18 (d18:1/18:0) ceramide, whilst CerS2 preferentially forms d18:1/24:0(C24:0) and d18:1/24:1 (C24:1) ceramides. CerS3 synthesizes very long chain ceramides (>C26-Cer), CerS4 forms C18-/C20-/C24-Cer; CerS5 and CerS6 synthesize mostly C14-/C16-/C18-Cer (48, 49). Thus, the broad spectrum of DhCer species accumulated first in the DEGS1 zebrafish model, and then reduced by fingolimod (spanning C13:1 DhCer to C28:0 DhCer, Supplemental Table 2), adds complexity to future studies aiming to identify the drug's most plausible targets in this model.

Additional experimental evidence supports the protective effect of FTY720 in sphingolipid metabolism-related disorders, such as GLD, which is caused by inactivation of galactosylceramidase (GALC) resulting in the accumulation of the toxic metabolite galactosylsphingosine (psychosine) in the brain. FTY720 treatment attenuated the psychosine-induced demyelination process in mouse organotypic cerebellar slice cultures (50). With this notion in mind, and our proof-of-principle results in a model organism, we posit that FTY720 (or novel, more specific next-generation sphingosine analogs interfering with CerS or other enzymatic steps along the

pathway may provide a promising therapeutic option for white matter disorders linked to *DEGS1* deficiency and perhaps others in sphingolipid metabolism, paving the way for the repurposing of FTY720 for other diseases. Our next step as a DEGS1-consortium is the validation of a robust biomarker in plasma (such as DhCer/Cer ratios) to monitor target engagement upon treatment and to prepare for early clinical intervention aiming to alleviate and modify disease course of this life-threatening condition.

Materials and methods

Patients, Genetic Studies and Ethics Statement

All 19 affected individuals underwent extensive clinical examination by a pediatric neurologist and at least one expert clinical geneticist at their referral hospitals, where broad metabolic and genetic testing was performed. Standardized phenotypic data were collected by review of the clinical histories and follow-up investigations (See Table 1-3). All available clinical and magnetic resonance image (MRI) data were collected and jointly reviewed. Whole-exome sequencing (WES) on an Illumina HiSeq platform were performed according to the following paradigms: (1) trio-based clinical diagnostic WES (individuals 1, 7, 9, 10, 11, 14, 17), (2) trio-based WES or trio-based WES plus affected sibling in a research-based analysis (individuals 3, 4, 15, 18, 19), or (3) WES of an affected individual followed by single site testing in parental DNA samples (individuals 6 and 8). Point mutations and indels were confirmed by Sanger sequencing of DNA sample from all available family members, when possible (Supplementary Table 3). The exome sequences have been deposited in public repositories: Patients 4 (phs000711.v5.p1), patients 13 (phs000744.v4.p2), and 18 (phs001272.v1.p1) into dbGaP; patient 1 (P0007232), patient 6 (P0005949), patient 7 (P0007704), patient 8 (P0007705), patient 9 (P0007706), patient 10 (P0007707), and patient 15 (P0007703) into Phenome Central.

Targeted Lipidomics Profiling

Briefly, cells were harvested using trypsin, and cell pellets contained 3·5 million cells. 50 mg muscle biopsy was snap frozen and stored at -80 °C until extraction. The zebrafish samples consisted of a pool of 5 zebrafish larvae (5 dpf) per experimental point (n=4) per condition. Lipidomics experiments were performed at Biocrates Life Science AG, as follows: Fibroblast cells were lysed by freeze-thaw cycles and metabolites were extracted with 60 µl ice-cold methanol. Zebrafish larvae were homogenized using Precellys and metabolites were extracted with 60 µl ice-cold methanol. For measuring metabolite concentrations from muscle tissue, the samples were first weighed and then homogenized using Precellys in methanol. Samples were centrifuged and the supernatant was used for further analysis. Ceramides, dihydroceramides, and 2-hydroxyacyl ceramides were quantitatively analyzed by high-throughput FIA-ESI-MS/MS. The reported lipid annotation represents a sum signal of all isobaric lipids with the same molecular weight (±0.5 Da range) within the same lipid

class. Multiple reaction monitoring (MRM) detection in positive and negative mode was performed using a SCIEX 4000 QTRAP® (SCIEX, Darmstadt, Germany) instrument. Sample preparation of 20 µL sample volume was followed by a MeOH/CHCl3-liquid/liquid-extraction protocol. In addition to five internal standards to compensate for matrix effects, 43 external standards were used for a multi-point calibration.The quantitative data analysis was performed with our in-house software MetIDQ™ enabling isotopic correction. We declare that all pre-analytical and analytical procedures were performed, documented and reviewed according to our ISO 9001:2008 certified in-house quality management rules and guidelines.

Zebrafish strains

Zebrafish embryos were obtained by mating of adult fish using standard methods. All fish strains were maintained individually as inbred lines. Wild type zebrafish strain was AB/Tu (RRID: ZIRC_ZL1/RRID: ZIRC_ZL57), and *Tg(mbp:egfp)* transgenic zebrafish was generated as described (27), in order to visualize myelinating oligodendrocytes in living zebrafish. Embryos were reared at 28·5 °C until processing for analyses at desired stages.

In situ hybridization and immunolabeling

Whole-mount in situ hybridization (ISH) was performed with standard protocols, as described previously (51). Embryos were fixed in 4% PFA, cryoprotected in 30% sucrose, and embedded in OCT. Blocks were frozen to improve tissue preservation, and then 10 µm sections were cut on a LeicaCM1510-1 cryostat (Leica). Hybridization was performed at 65°C with digoxigenin-labelled RNA probes. The antisense digoxigenin labelled RNA probe for zebrafish *degs1* (ENSDART00000013007.5) was generated by in vitro transcription of an amplicon from exon 1 (primers, forward 5'-ATG GGG AAC CGC GTG GCG CG -3'; reverse, 5'-TCA CTC CTG CTT GAC GTC TC -3'). Following purification, the fragment was cloned into a pBluescript dual promoter vector and was sequenced to confirm identity. The construct was linearized with BamHI, and digoxigenin-labelled antisense mRNA probe was generated by T3 in vitro transcription (DIG-RNA labelling kit, Roche 11-175-025-910). No signal was detected using the sense probe.

For GFP immunolabeling, staged embryos were fixed in 4 % paraformaldehyde (PFA) at room temperature for 20 min, washed in 0·1 % Tween 20/PBS, and incubated

overnight at 4 °C with anti-GFP primary antibody (GFP102; 1:500; Aves Labs) in blocking solution followed by secondary antibodies conjugated with Alexa Fluor 488. Sections were then washed three times in 1X PBS and mounted in Fluoromount (Sigma). Cryostat sections were imaged on a Nikon ECLIPSE 80i fluorescence microscope. ISH and fluorescent images were processed using ImageJ (National Institutes of Health, Bethesda, MD). Confocal images were acquired using a Leica TCS SL laser scanning confocal spectral microscope (Leica Microsystems Heidelberg GmbH, Mannheim, Germany). Calculation of the number of MBP + cells was performed using plugins in ImageJ software. We imaged a fixed area in the spinal cord (dotted box in Figure 5H). MBP^{+} cells (myelinating oligodendrocytes) were counted in the dorsal spinal cord of 4·5 dpf larvae.

Antisense morpholino injections

For morpholino knockdowns, embryos were injected with splice-blocking (sb) morpholino oligomers (MOs) obtained from GeneTools LLC (Philomath, OR). MO-*degs1*, 5′-GCT GAA TAA CTG CTC TCA CCA TTG G-3′ was designed as complementary to the genomic sequence flanking the exon 2-intron 2 boundary. Briefly, 1 nl of 5 ng/nl or 10 ng/nl MO-control and MO-DEGS1 were injected into the yolk of one-cell stage embryos. After injection embryos were incubated at 28·5ºC until the desired stage was reached. Injected embryos and uninjected clutch-mate controls were analyzed from 0 - 5 days post-fertilization (dpf). Every day dead larvae were removed and the fraction of surviving larvae was recorded till 5 dpf. In order to verify the efficiency of the morpholinos, RNA from uninjected, control MO and MO-DEGS1 injected larvae was extracted with Trizol (Thermo Fisher), and reverse transcription was performed with first-strand cDNA synthesis with the QuantiTect Reverse Transcription kit (Qiagen). The targeted region of *degs1* was PCR-amplified using primers complementary to sites in flanking exons located in exon 2 (5′- GGC TCT CTG AAC CTG CTG AC -3′) and exon 3 (5′CTT GAC GTC TCC GAC CAG TT-3′), respectively using standard PCR conditions (Ta: 60 °C), and migrated by electrophoresis on a 1 % agarose gel; bands were excised, gel purified using QIAquick gel extraction kit (Qiagen) and resulting clones were Sanger sequenced to confirm aberrant splicing events induced by the MO (Supplementary Figure 4G-I). The standard

MO-control against β-globin was also obtained from GeneTools (5′-CCT CTT ACC TCA GTT ACA ATT TAT A-3′) was used as negative control.

Larval Locomotor Behavior Assay

By 5 dpf, zebrafish larvae perform spontaneous swimming and their visual system is fully developed. Uninjected, MO control and MO-DEGS1 120 hpf (hours post fertilization) larvae were transferred to individual wells of 96-well plate with 150 µl fresh fish water and allowed to acclimate for a few hours. The zebrafish larvae behaviour is tracked and analysed by the EthoVision XT software and the DanioVision device from Noldus Information Technologies, Wageningen, The Netherlands. This closed system consists of a camera placed above a chamber with circulating water and a temperature sensor that is set at 28·5 ºC. Individualized larvae in a 96-wells plate are placed in the chamber, which can provide different stimuli (light/dark environment, tapping, sound) controlled by the software. Prior to each experiment, larvae were left for 10 minutes in dark for acclimation, then predetermined series of alternating dark and light environment are presented to the larvae. The natural locomotor behaviour of zebrafish larvae is characterized by high activity in darkness and immobility in light environments. The final 25 min long experimental protocol is divided in 5 min period of darkness, and then two times repeated cycle of 5 min of bright light followed by 5 min of darkness. During the behavioural trial the total distance moved by every larva is measured. We obtained the distance moved and the mobility parameters from EthoVision tracking program analysis, and baseline parameters were subtracted out before. All locomotor assays were performed at 1pm onwards to ensure steady activity of zebrafish (52). After observations, all subjects were euthanized with a lethal concentration of MS-222 Tricaine (ethyl-3-aminobenzoate methane-sulfonate salt; Sigma). Swimming behaviour after drug treatment was performed by adding FTY720 to standard fish water to the final concentration of 3·3, 1·0, 0·3 ng/µl. DMSO was used as vehicle. MO control and MO-DEGS1 embryos (0 hpf) were treated with FTY720 till 120 hpf and behavior assay was performed as described above. All measures were averaged across larvae within each condition (n = 20 larvae/condition) and reported as population means ± SD.

Statistical analysis

All experiments were repeated at least 3 times with consistent results. All cell culture data were from biologic triplicates, unless otherwise indicated. Statistical analysis was performed with two-tailed unpaired Student's t test (*P < 0.05, ** P < 0.01, *** P < 0.001), for comparison of 2 groups, and ANOVA followed by Tukey's post hoc test for multiple comparisons (*P < 0.05, ** P < 0.01, *** P < 0.001) after verifying normality. Statistical analyses were performed using the GraphPad Prism 7.0 program.

Study approval

Human study:

Human genetic studies conducted in research laboratories were approved by local ethics committees from participating centers (Barcelona, Spain (IDIBELL: PR076/14); Paris, France (INSERM U1163: 2015-03-03/DC 2014-2272; LEUKOFRANCE: CPP AU788; CNIL 1406552; AFSSAPS B90298-60); California, US (University of California, San Diego: IRB 140028), (Peking, China (Peking University First Hospital: [2005]004), Rochester, US (Mayo Clinic: IRB 12-009346), Baltimore, US (Johns Hopkins School of Medicine: NA_00045758); Hamilton, Canada; Ahvaz, Iran (Shahid Chamran University of Ahvaz: EE/97.24.3 17654/scu.ac.ir). Parental (or legal guardian) written informed consent was obtained for all affected children. Written informed consent was provided for the video appearing in supplementary data.

Zebrafish study:

All protocols used have been approved by the Institutional Animal Care and Use Ethic Committee (PRBB–IACUEC) and implemented according to national and European regulations. All experiments were carried out in accordance with the principles of the 3Rs.

Authors'contributions

DP, NL, SF, JJ, MR, CCo, DR, JT and CP performed and/or interpreted or supervised aspects of the different experiments. SAA, MEY, CC, MJW, DV, GL, KSP, IDe, HY, JW, MB, LB, MT, KNJ, DM, MSZ, MCP, BCL, EWK, FPV, EW, NLMS, JSC, RM, HG, NM, GS, LC, DRo, JGG, AF, OBT undertook clinical and genealogical studies and provided clinical data and biological specimens from patients. ID and AS undertook variant calling and bioinformatic analyses on whole exome sequencing data. DP and AP analyzed and interpreted data and wrote the initial draft of the manuscript. OBT supervised the clinical and MRI data in coordination with AP. AP provided overall study direction, funding, coordination, supervision, and revised the manuscript. All authors critically reviewed the report and approved the final version.

Supplementary Data

Supplementary Data include material and methods, 4 Figures, 3 tables and 1 video.

Acknowledgements

We thank CERCA Program/ Generalitat de Catalunya for institutional support. We also thank Juanjo Martínez and Cristina Guilera for excellent technical assistance and Asociación Española contra las Leucodistrofias (ALE-ELA España). We are indebted to the NIH NeuroBioBank for supplying the case material used for the human studies. The authors thank the affected individuals and their families for participation in this study. This study was supported by the ISCIII [FIS PI14/00581] (Co-funded by European Regional Development Fund. ERDF, a way to build Europe) , 'La Marató de TV3' Foundation 345/C/2014 (to **A.P., CC and C.P**.), the Hesperia Foundation and CIBER on Rare Diseases (CIBERER) [ACCI14-759] and the Secretariat for Universities and Research of the Ministry of Business and Knowledge of the Government of Catalonia [2017SGR1206] to **A.P**.; Spanish Ministry of Economy and Competitiveness (MINECO-FEDER): BFU2015-67400-P to **C.P**., the Spanish Institute for Health Carlos III [Miguel Servet program CPII16/00016] to **S.F**. and the Center for Biomedical Research on Rare Diseases (CIBERER) to **N.L**. and **M.R**., and a predoctoral fellowship awarded from the Government of Catalonia through L´Agència de Gestió d'Ajuts Universitaris i de Recerca (AGAUR; FI-DGR 2014) to **D. P. X.J.** acknowledges a Sara Borrell postdoctoral fellowship from Instituto de Salud Carlos III. Grants to **L.C**.: National Research Agency (ANR-10-IAHU-01) and Fondation pour la Recherche

Médicale (DEQ20160334938). The authors thank the members of LEUKOFRANCE, particularly the Biobank in Clermont Ferrand (Eleonore Pierre and Philippe Vago) and Kremlin Bicetre (Elise Lebigot and Abdelhamid Slama) University Hospitals. Grants to **OBT**: European Union FP7 RD- Connect project, ELA Foundation (2009-007I4AV2) and "Les amis de Ianis" association (Ploudaniel, France). **ID** was supported by an ELA grant and is currently supported by the RD-connect project. **M.J.W**.: The views expressed herein are my own and do not necessarily reflect the official policy or position of the Department of the Navy, Department of Defense, or the U.S. Government. **J.G.G:** NIH grants P01HD070494, 1R01NS098004, R01NS048453, R01NS052455, and UL1TR001866 from the National Center for Advancing Translational Sciences (NCATS), National Institutes of Health (NIH) Clinical and Translational Science Award (CTSA) program, the Simons Foundation Autism Research Initiative (275275), Howard Hughes Medical Institute, Qatar National Research Foundation NPRP 6-1463-3-351. We thank Yale University Center for Mendelian Genomics (Mark Gerstein, Murat Gunel, Richard P. Lifton, Shrikant M. Mane, 5UM1HG006504) and the Broad Institute (Daniel G. MacArthur and Heidi L Rehm, 5UM1HG008900) for sequencing support.

NS: National Institutes of Health grant 1U54 HG006542. The Baylor-Hopkins Center for Mendelian Genomics and GeneMatcher are supported by a grant from the National Human Genome Research Institute, 1U54HG006493.

AF: Grants from the Kennedy Krieger Institute Intellectual and Developmental Disabilities Research Center grant (funded through NICHD U54 HD079123).

MB: National Institutes of Health grants NS056780 (MB) and the National Ataxia Foundation. MCP: Grants from the National Institutes of Health (NS 65768-01), the Peggy Furth Fund, the National MS Society. **EWK:** Mayo Clinic Center for Individualized Medicine (CIM), the Investigative and Functional Genomics Program and the William O. Lund, Jr. and Natalie C. Lund Charitable Foundation. **MAT:** Genetic testing was performed under the Care4Rare Canada Consortium funded by Genome Canada, the Canadian Institutes of Health Research, the Ontario Genomics Institute, Ontario Research Fund, Genome Quebec and Children's Hospital of Eastern Ontario Foundation. We wish to acknowledge the contribution of the high throughput sequencing platform of the McGill University and Génome Québec Innovation Centre, Montréal, Canada. We are grateful to Dr. Cheol-Hee Kim for providing the Tol2

transposon vector, Bellvitge Biobank for providing control human muscle tissues. AP and EWK are members of the Undiagnosed Diseases Program International (UDNI).

Conflict of Interest

The authors declare that this article was conducted in the absence of any commercial or financial relationships that could be construed as a potential conflict of interest.

URLs

1000 Genomes, http://phase3browser.1000genomes.org/index.html
CADD, http://cadd.gs.washington.edu/
Clustalw, http://www.clustal.org/
Database of Genomic Variants, http://dgv.tcag.ca/dgv/app/home/
DECIPHER, https://decipher.sanger.ac.uk/
Ensembl Genome Browser, https://www.ensembl.org/index.html
EVS, http://evs.gs.washington.edu/EVS/
Exac Browser, http://exac.broadinstitute.org/
Fiji, https://fiji.sc/
GATK, https://software.broadinstitute.org/gatk/
Genbank, http://www.ncbi.nlm.nih.gov/genbank/
Genematcher, https://genematcher.org/
GME Variome (http://igm.ucsd.edu/gme/)
Gnomad browser, http://gnomad.broadinstitute.org/
Graphpad, https://www.graphpad.com/
HGVS, http://varnomen.hgvs.org
Human Genotype-Tissue Expression portal https://www.gtexportal.org
Iranome (http://www.iranome.ir/) GME Variome (http://igm.ucsd.edu/gme/)
Mouse brain atlas http://mouse.brain-map.org/
NHLBI Exome Sequencing Project (ESP) Exome Variant Server, http://evs.gs.washington.edu/EVS/
OMIM, http://www.omim.org/
Polyphen-2, http://genetics.bwh.harvard.edu/pph2/
Primer3, http://bioinfo.ut.ee/primer3
SIFT, http://sift.bii.a-star.edu.sg/
SNP, https://www.ncbi.nlm.nih.gov/snp
The Human Protein Atlas, http://www.proteinatlas.org/
UCSC Genome Browser, http://genome.ucsc.edu
Uniprot, http://www.uniprot.org/
Zfin, https://zfin.org

References

1. Kohler, W., Curiel, J., and Vanderver, A. 2018. Adulthood leukodystrophies. *Nat Rev Neurol* 14:94-105.
2. Parikh, S., Bernard, G., Leventer, R.J., van der Knaap, M.S., van Hove, J., Pizzino, A., McNeill, N.H., Helman, G., Simons, C., Schmidt, J.L., et al. 2015. A clinical approach to the diagnosis of patients with leukodystrophies and genetic leukoencephelopathies. *Mol Genet Metab* 114:501-515.
3. van der Knaap, M.S., and Bugiani, M. 2017. Leukodystrophies: a proposed classification system based on pathological changes and pathogenetic mechanisms. *Acta Neuropathol* 134:351-382.
4. Dorboz, I., Aiello, C., Simons, C., Stone, R.T., Niceta, M., Elmaleh, M., Abuawad, M., Doummar, D., Bruselles, A., Wolf, N.I., et al. 2017. Biallelic mutations in the homeodomain of NKX6-2 underlie a severe hypomyelinating leukodystrophy. *Brain* 140:2550-2556.
5. Edvardson, S., Yi, J.K., Jalas, C., Xu, R., Webb, B.D., Snider, J., Fedick, A., Kleinman, E., Treff, N.R., Mao, C., et al. 2016. Deficiency of the alkaline ceramidase ACER3 manifests in early childhood by progressive leukodystrophy. *J Med Genet* 53:389-396.
6. Mendes, M.I., Gutierrez Salazar, M., Guerrero, K., Thiffault, I., Salomons, G.S., Gauquelin, L., Tran, L.T., Forget, D., Gauthier, M.S., Waisfisz, Q., et al. 2018. Bi-allelic Mutations in EPRS, Encoding the Glutamyl-Prolyl-Aminoacyl-tRNA Synthetase, Cause a Hypomyelinating Leukodystrophy. *Am J Hum Genet* 102:676-684.
7. Eichler, F., Duncan, C., Musolino, P.L., Orchard, P.J., De Oliveira, S., Thrasher, A.J., Armant, M., Dansereau, C., Lund, T.C., Miller, W.P., et al. 2017. Hematopoietic Stem-Cell Gene Therapy for Cerebral Adrenoleukodystrophy. *N Engl J Med* 377:1630-1638.
8. Ferreira, C.R., and Gahl, W.A. 2017. Lysosomal storage diseases. *Transl Sci Rare Dis* 2:1-71.
9. Endo, K., Akiyama, T., Kobayashi, S., and Okada, M. 1996. Degenerative spermatocyte, a novel gene encoding a transmembrane protein required for the initiation of meiosis in Drosophila spermatogenesis. *Mol Gen Genet* 253:157-165.
10. Ternes, P., Franke, S., Zahringer, U., Sperling, P., and Heinz, E. 2002. Identification and characterization of a sphingolipid delta 4-desaturase family. *J Biol Chem* 277:25512-25518.
11. Hannun, Y.A., and Obeid, L.M. 2011. Many ceramides. *J Biol Chem* 286:27855-27862.
12. Montefusco, D.J., Chen, L., Matmati, N., Lu, S., Newcomb, B., Cooper, G.F., Hannun, Y.A., and Lu, X. 2013. Distinct signaling roles of ceramide species in yeast revealed through systematic perturbation and systems biology analyses. *Sci Signal* 6:rs14.
13. Rodriguez-Cuenca, S., Barbarroja, N., and Vidal-Puig, A. 2015. Dihydroceramide desaturase 1, the gatekeeper of ceramide induced lipotoxicity. *Biochim Biophys Acta* 1851:40-50.
14. Schmitt, S., Castelvetri, L.C., and Simons, M. 2015. Metabolism and functions of lipids in myelin. *Biochim Biophys Acta* 1851:999-1005.
15. Yeh, Y.Y. 1988. Long chain fatty acid deficits in brain myelin sphingolipids of undernourished rat pups. *Lipids* 23:1114-1118.

16. Hannun, Y.A., and Obeid, L.M. 2018. Sphingolipids and their metabolism in physiology and disease. *Nat Rev Mol Cell Biol* 19:175-191.
17. Di Pardo, A., Basit, A., Armirotti, A., Amico, E., Castaldo, S., Pepe, G., Marracino, F., Buttari, F., Digilio, A.F., and Maglione, V. 2017. De novo Synthesis of Sphingolipids Is Defective in Experimental Models of Huntington's Disease. *Front Neurosci* 11:698.
18. Fonteh, A.N., Ormseth, C., Chiang, J., Cipolla, M., Arakaki, X., and Harrington, M.G. 2015. Sphingolipid metabolism correlates with cerebrospinal fluid Beta amyloid levels in Alzheimer's disease. *PLoS One* 10:e0125597.
19. Holland, W.L., Brozinick, J.T., Wang, L.P., Hawkins, E.D., Sargent, K.M., Liu, Y., Narra, K., Hoehn, K.L., Knotts, T.A., Siesky, A., et al. 2007. Inhibition of ceramide synthesis ameliorates glucocorticoid-, saturated-fat-, and obesity-induced insulin resistance. *Cell Metab* 5:167-179.
20. Jung, W.H., Liu, C.C., Yu, Y.L., Chang, Y.C., Lien, W.Y., Chao, H.C., Huang, S.Y., Kuo, C.H., Ho, H.C., and Chan, C.C. 2017. Lipophagy prevents activity-dependent neurodegeneration due to dihydroceramide accumulation in vivo. *EMBO Rep* 18:1150-1165.
21. Sobreira, N., Schiettecatte, F., Valle, D., and Hamosh, A. 2015. GeneMatcher: a matching tool for connecting investigators with an interest in the same gene. *Hum Mutat* 36:928-930.
22. Steenweg, M.E., Vanderver, A., Blaser, S., Bizzi, A., de Koning, T.J., Mancini, G.M., van Wieringen, W.N., Barkhof, F., Wolf, N.I., and van der Knaap, M.S. 2010. Magnetic resonance imaging pattern recognition in hypomyelinating disorders. *Brain* 133:2971-2982.
23. Lopez-Erauskin, J., Galino, J., Ruiz, M., Cuezva, J.M., Fabregat, I., Cacabelos, D., Boada, J., Martinez, J., Ferrer, I., Pamplona, R., et al. 2013. Impaired mitochondrial oxidative phosphorylation in the peroxisomal disease X-linked adrenoleukodystrophy. *Hum Mol Genet* 22:3296-3305.
24. Enomoto, A., Omae, F., Miyazaki, M., Kozutsumi, Y., Yubisui, T., and Suzuki, A. 2006. Dihydroceramide:sphinganine C-4-hydroxylation requires Des2 hydroxylase and the membrane form of cytochrome b5. *Biochem J* 397:289-295.
25. Omae, F., Miyazaki, M., Enomoto, A., and Suzuki, A. 2004. Identification of an essential sequence for dihydroceramide C-4 hydroxylase activity of mouse DES2. *FEBS Lett* 576:63-67.
26. Czopka, T. 2016. Insights into mechanisms of central nervous system myelination using zebrafish. *Glia* 64:333-349.
27. Jung, S.H., Kim, S., Chung, A.Y., Kim, H.T., So, J.H., Ryu, J., Park, H.C., and Kim, C.H. 2010. Visualization of myelination in GFP-transgenic zebrafish. *Dev Dyn* 239:592-597.
28. Baraban, S.C., Dinday, M.T., and Hortopan, G.A. 2013. Drug screening in Scn1a zebrafish mutant identifies clemizole as a potential Dravet syndrome treatment. *Nat Commun* 4:2410.
29. Lahiri, S., Park, H., Laviad, E.L., Lu, X., Bittman, R., and Futerman, A.H. 2009. Ceramide synthesis is modulated by the sphingosine analog FTY720 via a mixture of uncompetitive and noncompetitive inhibition in an Acyl-CoA chain length-dependent manner. *J Biol Chem* 284:16090-16098.
30. The Lancet, N. 2017. Rare advances for rare diseases. *Lancet Neurol* 16:1.
31. Tonduti, D., Aiello, C., Renaldo, F., Dorboz, I., Saaman, S., Rodriguez, D., Fettah, H., Elmaleh, M., Biancheri, R., Barresi, S., et al. 2016. TUBB4A-related

hypomyelinating leukodystrophy: New insights from a series of 12 patients. *Eur J Paediatr Neurol* 20:323-330.
32. Sarret, C., Lemaire, J.J., Tonduti, D., Sontheimer, A., Coste, J., Pereira, B., Feschet, F., Roche, B., and Boespflug-Tanguy, O. 2016. Time-course of myelination and atrophy on cerebral imaging in 35 patients with PLP1-related disorders. *Dev Med Child Neurol* 58:706-713.
33. Sandhoff, K., and Christomanou, H. 1979. Biochemistry and genetics of gangliosidoses. *Hum Genet* 50:107-143.
34. Kohlschutter, A. 2013. Lysosomal leukodystrophies: Krabbe disease and metachromatic leukodystrophy. *Handb Clin Neurol* 113:1611-1618.
35. Hernandez-Tiedra, S., Fabrias, G., Davila, D., Salanueva, I.J., Casas, J., Montes, L.R., Anton, Z., Garcia-Taboada, E., Salazar-Roa, M., Lorente, M., et al. 2016. Dihydroceramide accumulation mediates cytotoxic autophagy of cancer cells via autolysosome destabilization. *Autophagy* 12:2213-2229.
36. Siddique, M.M., Li, Y., Chaurasia, B., Kaddai, V.A., and Summers, S.A. 2015. Dihydroceramides: From Bit Players to Lead Actors. *J Biol Chem* 290:15371-15379.
37. Ruiz, M., Begou, M., Launay, N., Ranea-Robles, P., Bianchi, P., Lopez-Erauskin, J., Morato, L., Guilera, C., Petit, B., Vaurs-Barriere, C., et al. 2018. Oxidative stress and mitochondrial dynamics malfunction are linked in Pelizaeus-Merzbacher disease. *Brain Pathol* 28:611-630.
38. Kraveka, J.M., Li, L., Szulc, Z.M., Bielawski, J., Ogretmen, B., Hannun, Y.A., Obeid, L.M., and Bielawska, A. 2007. Involvement of dihydroceramide desaturase in cell cycle progression in human neuroblastoma cells. *J Biol Chem* 282:16718-16728.
39. Olsen, A.S.B., and Faergeman, N.J. 2017. Sphingolipids: membrane microdomains in brain development, function and neurological diseases. *Open Biol* 7:1-17.
40. Chami, M., Halmer, R., Schnoeder, L., Anne Becker, K., Meier, C., Fassbender, K., Gulbins, E., and Walter, S. 2017. Acid sphingomyelinase deficiency enhances myelin repair after acute and chronic demyelination. *PLoS One* 12:e0178622.
41. Penno, A., Reilly, M.M., Houlden, H., Laura, M., Rentsch, K., Niederkofler, V., Stoeckli, E.T., Nicholson, G., Eichler, F., Brown, R.H., Jr., et al. 2010. Hereditary sensory neuropathy type 1 is caused by the accumulation of two neurotoxic sphingolipids. *J Biol Chem* 285:11178-11187.
42. Ruiz, M., Jove, M., Schluter, A., Casasnovas, C., Villarroya, F., Guilera, C., Ortega, F.J., Naudi, A., Pamplona, R., Gimeno, R., et al. 2015. Altered glycolipid and glycerophospholipid signaling drive inflammatory cascades in adrenomyeloneuropathy. *Hum Mol Genet* 24:6861-6876.
43. Brunkhorst, R., Vutukuri, R., and Pfeilschifter, W. 2014. Fingolimod for the treatment of neurological diseases-state of play and future perspectives. *Front Cell Neurosci* 8:283.
44. Miron, V.E., Jung, C.G., Kim, H.J., Kennedy, T.E., Soliven, B., and Antel, J.P. 2008. FTY720 modulates human oligodendrocyte progenitor process extension and survival. *Ann Neurol* 63:61-71.
45. Gurevich, M., Waknin, R., Stone, E., and Achiron, A. 2018. Fingolimod-improved axonal and myelin integrity of white matter tracts associated with multiple sclerosis-related functional impairments. *CNS Neurosci Ther* 24:412-419.

46. Levy, M., and Futerman, A.H. 2010. Mammalian ceramide synthases. *IUBMB Life* 62:347-356.
47. Brondolin, M., Berger, S., Reinke, M., Tanaka, H., Ohshima, T., Fubeta, B., and Hoch, M. 2013. Identification and expression analysis of the zebrafish homologs of the ceramide synthase gene family. *Dev Dyn* 242:189-200.
48. Ben-David, O., and Futerman, A.H. 2010. The role of the ceramide acyl chain length in neurodegeneration: involvement of ceramide synthases. *Neuromolecular Med* 12:341-350.
49. Mizutani, Y., Kihara, A., and Igarashi, Y. 2005. Mammalian Lass6 and its related family members regulate synthesis of specific ceramides. *Biochem J* 390:263-271.
50. O'Sullivan, C., and Dev, K.K. 2015. Galactosylsphingosine (psychosine)-induced demyelination is attenuated by sphingosine 1-phosphate signalling. *J Cell Sci* 128:3878-3887.
51. Sapede, D., Dyballa, S., and Pujades, C. 2012. Cell lineage analysis reveals three different progenitor pools for neurosensory elements in the otic vesicle. *J Neurosci* 32:16424-16434.
52. MacPhail, R.C., Brooks, J., Hunter, D.L., Padnos, B., Irons, T.D., and Padilla, S. 2009. Locomotion in larval zebrafish: Influence of time of day, lighting and ethanol. *Neurotoxicology* 30:52-58.

Figure legends

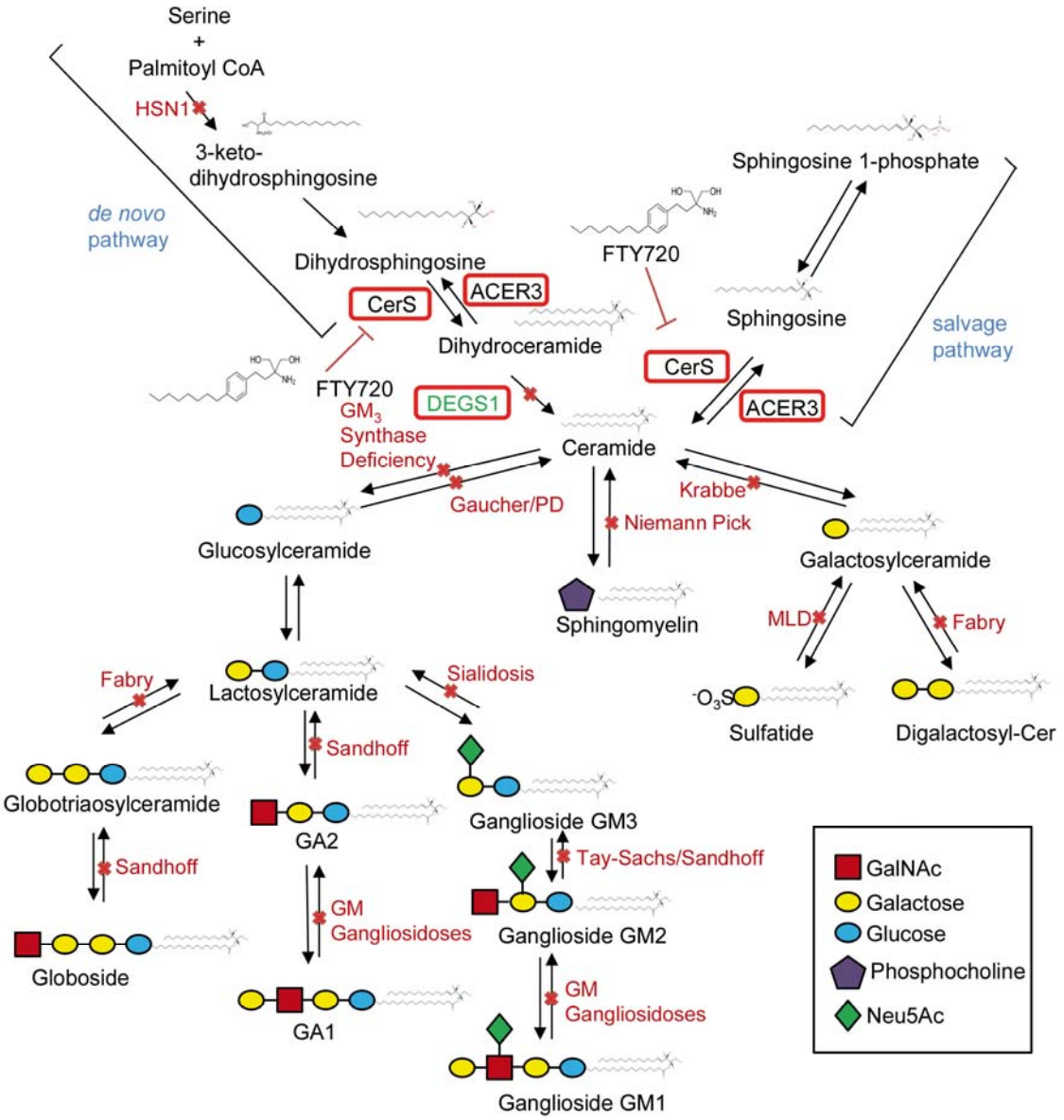

Figure. 1. **Scheme depicting enzyme defects associated with neurological disorders in the sphingolipid metabolism pathway, and Fingolimod (FTY720) action**. Serine palmitoyltransferase (SPT) catalyzes the initial reaction of the *de novo* sphingolipid pathway. Dihydrosphingosine is produced after an intermediate step regulated by 3-keto-dihydrosphingosine reductase (KDS), which is then followed by acylation by ceramide synthase (CerS) to produce dihydroceramide. The final reaction is the addition of a double bond by dihydroceramide desaturase DEGS1 to form ceramide. Ceramide is metabolized by ceramidase (CDse) to generate sphingosine, which in turn produces sphingosine 1-phosphate through phosphorylation by sphingosine kinase-1 and sphingosine kinase-2 (SphK1/2). Sphingosine 1-phosphate can be catabolized into hexadecenal and ethanolamine phosphate by sphingosine 1-phosphate lyase (S1PL).

Ceramide can be generated by the breakdown of sphingomyelin (SM) by acid (ASM) or neutral sphingomyelinases (NSM). Fingolimod (FTY720) has inhibitory effects on CerS. Enzyme (in bold) defects are indicated by solid bars across the blue arrows. The names of diseases are given (red box). SPT, serine palmitoyltransferase; KDS, 3-keto-dihydrosphingosine reductase; CerS, ceramide synthase; DEGS1, dihydroceramide desaturase; HSN1, hereditary sensory neuropathy type I; MLD, metachromatic leukodystrophy; PD, Parkinson disease; GalCer, galactosylceramide; Sap, saposin.

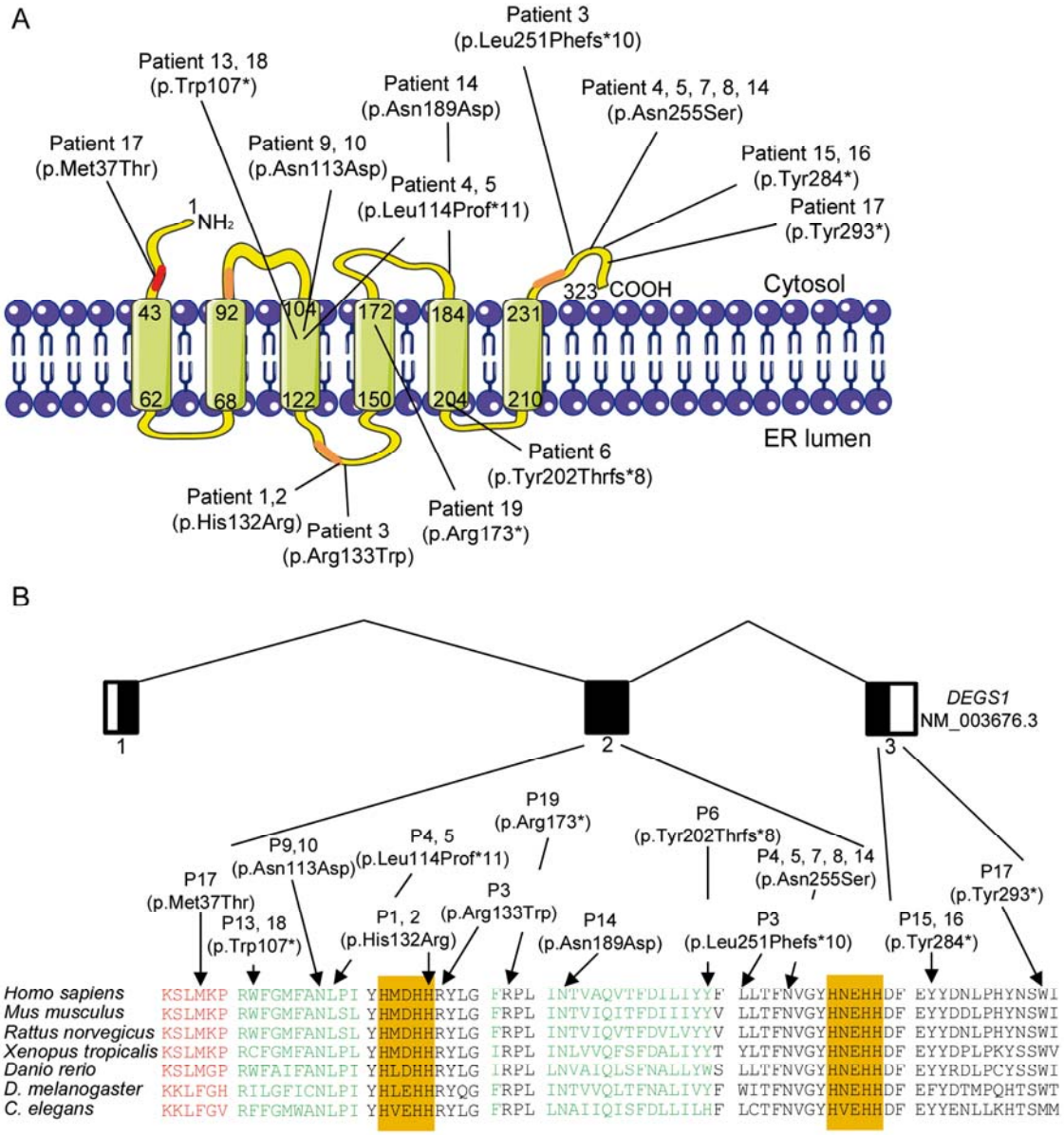

Figure 2. Schematic representation of human DEGS1 (NP_003667.1) and its functional domains with variants identified in patients. (A) DEGS1 has 323 amino acids. Numbers under the protein line indicate the boundaries of each domain. The lipid

DES domain (red) of DEGS1 comprises amino acids 6-42. The histidine domain (orange) of DEGS1 comprises amino acids 89-93, 128-132, and 259-263. The transmembrane domain (green) of DEGS1 comprises amino acids 43-62, 68-92, 104-122, 150-172, 184-202, and 210-231. The fatty acid desaturase (FAD) domain covers amino acids 64-293. Multiple protein sequence alignment of DEGS1 orthologs show conservation of missense mutations detected in cases (bottom). (B) Schematic of the human *DEGS1* locus which consists of three exons. The alignment was performed from different species is shown (bottom). The lipid DES, transmembrane and histidine domain are indicated by red, green and orange shading respectively. The alignment was performed with ClustalW using the following RefSeq numbers: NP_003667.1, Homo sapiens; NP_031879.1, Mus musculus; NP_445775.2, Rattus norvegicus; NP_001007485.1, Xenopus tropicalis; NP_997865.1, Danio rerio; NP_476594.1, Drosophila melanogaster; NP_493549.1, Caenorhabditis elegans.

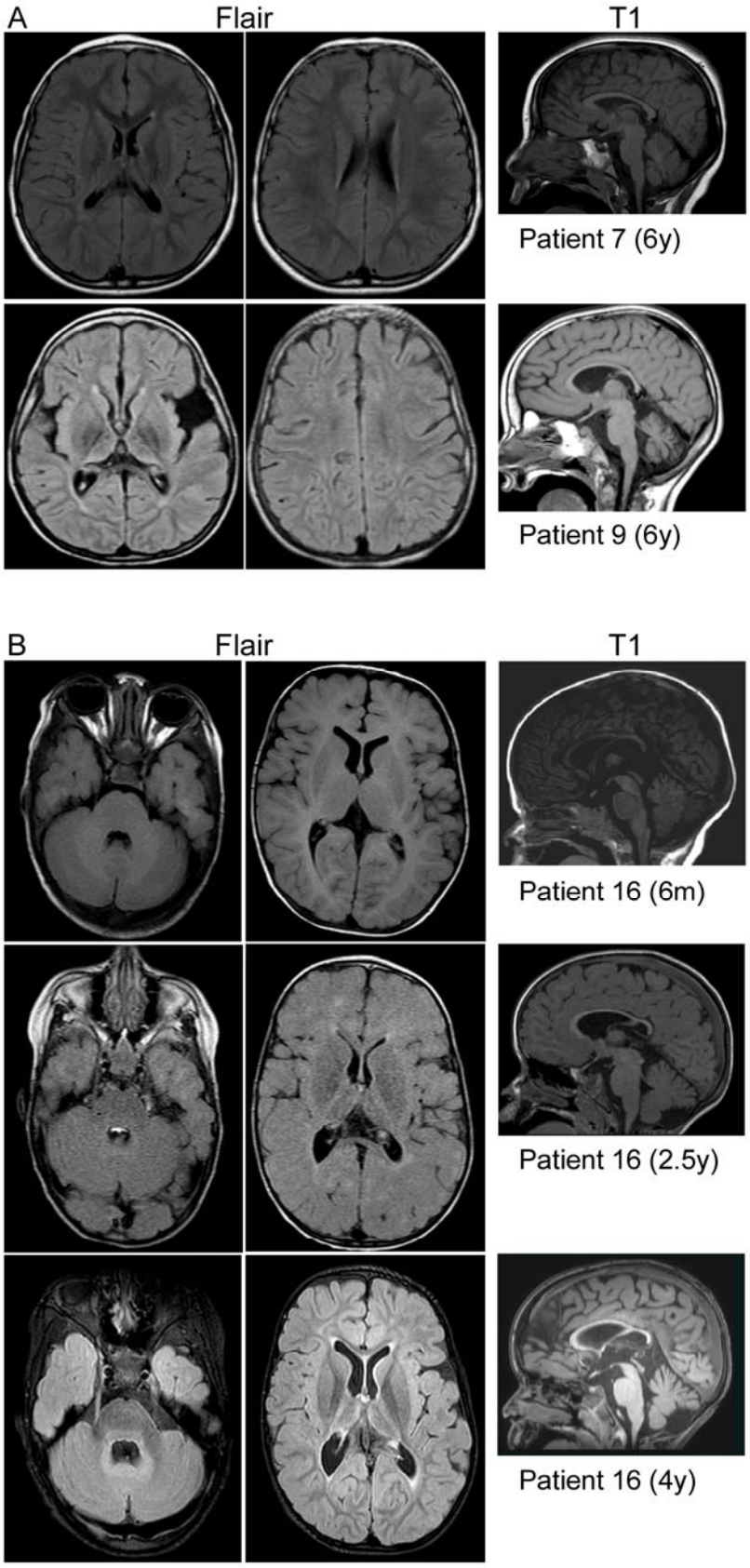

Figure 3. Brain MRIs according to clinical severity and follow up.

(A) MRIs of patients with distinct clinical severity at the age of 6 years. Patient 7 (Top row) shows the mildest presentation with walking acquisition and spastic paraplegia. In FLAIR sequences, mild hyperintensities of the periventricular white matter (WM), with normal CC and internal capsule. In T1 sagittal, normal cerebellum and CC. Patient 9 (low row) was able to hold the head but develop dystonia and spasticity with failure to thrive (-4SD). Despite this severe clinical presentation, the FLAIR sequences show an abnormal hypersignal of the white matter only in the periventricular and deep regions that are atrophic. The CC and the cerebellar vermis are atrophic.

(B) Sequencial MRIs of patient 16. At 6 months all the WM structures including the cerebellum, the brainstem and the CC appear unmyelinated. The CC is thin on the T1 sagittal section. A progression in the myelination has occurred at 2.5 y of age but the posterior part of the internal capsules is not myelinated, with periventricular hypersignals and an isosignal of the deep and subcortical WM and atrophic thalami. At 4 years of age the internal capsules, the deep and subcortical WM show normal myelinated signal whereas the thalami appeared in hypersignal and atrophic, as well as the cerebellar vermis.

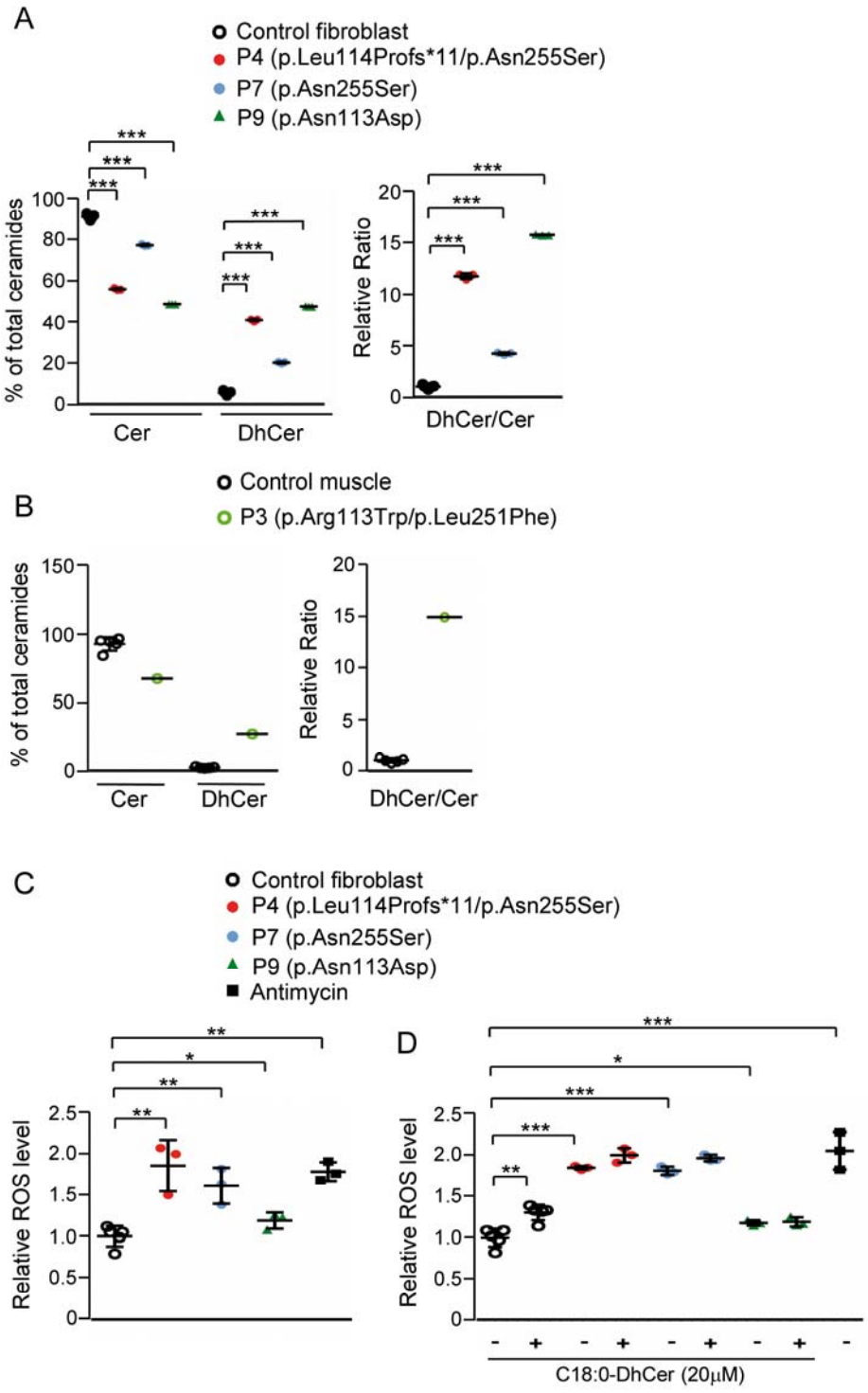

Figure 4. Dihydroceramides and ceramides imbalance in human patient fibroblasts (P4, P7, P9) and muscle (P3). (A) Ceramides (Cer), dihydroceramides (DhCer), and the ratios DhCer/Cer in human controls (n=9) and patient fibroblasts $(n=3)^{+}$ and (B) in human controls (n=5) and patient muscle (n=1). Data are represented as percentage of total ceramides and dihydroceramides. (C) Intracellular ROS was quantified using the H_2DCFDA probe in patient fibroblasts (patients 4, 7 and 9) and

controls (n=5) at a basal level^{+} (D) Exogenous DhCer (C18:0) treatment (20 µM, 6h) was applied to control and patient's fibroblasts. Antimycin was used as positive control for ROS generation^{++}. The fibroblasts results are from three independent experiments and they have been performed in triplicate. Data are shown as the means ± SD * p<0·05; ** p<0·01; *** p<0·001 after one-way ANOVA^{+} or two-way ANOVA^{++} test followed by Tukey's post hoc test.

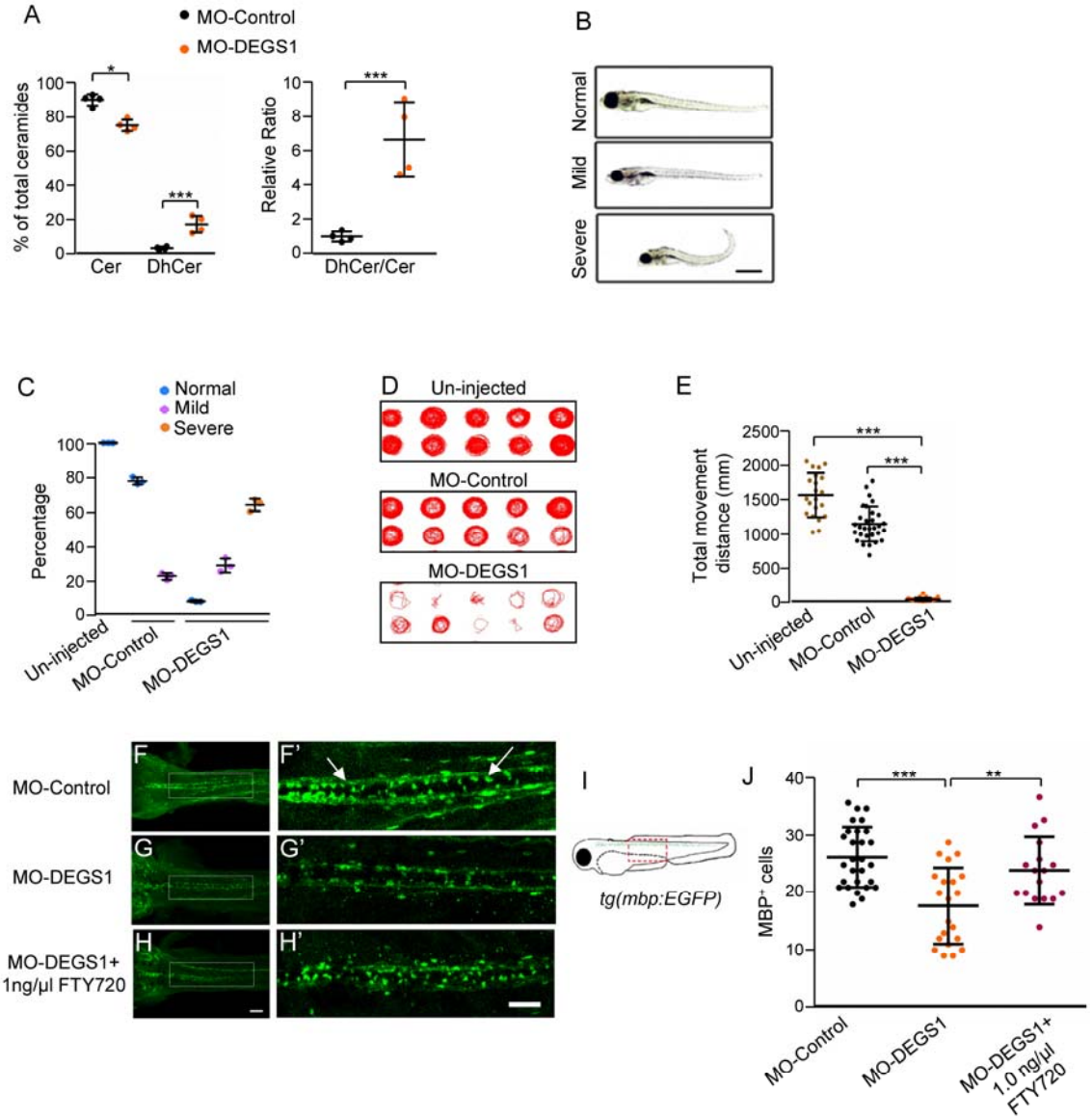

Figure 5. Impact of *Degs1* knockdown in *Danio rerio* larvae

(A) Ceramides (Cer), dihydroceramides (DhCer), and the ratios DhCer/Cer in zebrafish MO-control and MO-DEGS1, n=4/condition (5 larvae per tube/condition), at 5 dpf^{+}. Data are represented as percentage of total ceramides and dihydroceramides. (B) Representative images of the normal (blue), mild (purple), and severe (orange) phenotypes observed in the control and MO-DEGS1 injected groups. Scale bar: 10 µm.

(C) Quantification at 5 dpf of the percentage of normal, mild, and severe phenotype groups obtained. Values are the percentage ± SD of the three independent experiments with n = 50 animals per group per experiments. (D) Examples of digital tracks of 10 single larvae of each condition shown in red. (E) Scatter plot displaying the total movement distance by different larvae (uninjected larvae (n=20): 1564·4 mm ± 321·6, MO-control (n=30): 1146·6 mm ± 255·2, MO-DEGS1 (n=33): 28·3 mm ± 24·5)$^{++}$. (F-H) Dorsal views of larvae injected with control and MO-DEGS1, and (F'-H') inserts of boxed areas at 4·5 dpf. Scale bar: 100 µm. White arrows indicate MBP^{+} cells (myelinating oligodendrocytes). (I) Illustration of the *tg(mbp:EGFP)* larvae. (J) Scatter plot displaying the number of MBP^{+} in the dorsal spinal cord of 4·5 dpf larvae (MO-control: n=30, MO-DEGS1*:* n=28, MO-DEGS1+1 ng/µl FTY720: n=19)$^{++}$. Data are shown as the means ± SD; * p<0·05; ** p<0·01; *** p<0·001 after two-tailed unpaired Student's t test^{+} or one-way ANOVA^{++} test followed by Tukey's post hoc test.

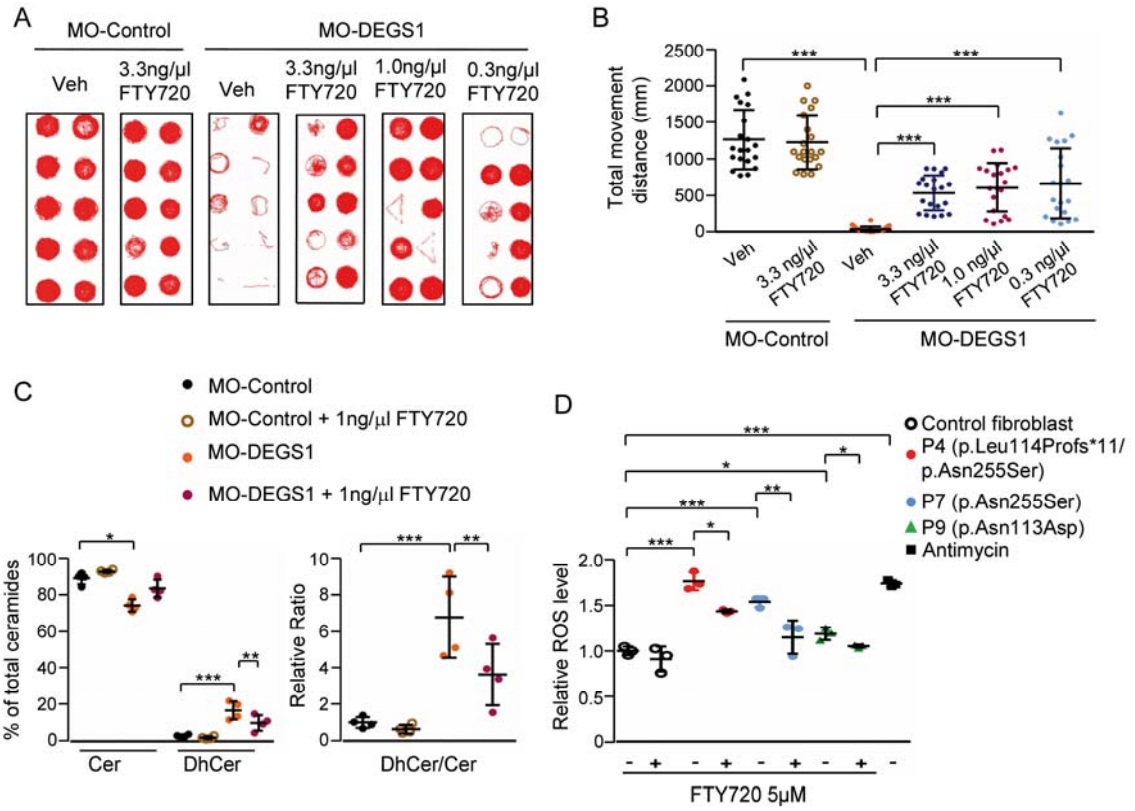

Figure 6. FTY720 ameliorates locomotor, biochemical and cellular phenotype in MO-DEGS1 larvae and lowers ROS levels in patient's fibroblasts. (A) MO-DEGS1 larvae were treated for 120 h with fingolimod (FTY720) at 0·3, 1·0 and 3·3 ng/µl. Digital tracks of larvae are shown in red. (B) Scatter plot (n=20 by condition) showing total movement distance (mm) upon FTY720 treatment^{++}. Total movement distance

(mm) traveled by MO control (veh. 1268·2 mm ± 402·9); (FTY720, 1230 mm ± 365·2); compared to MO-DEGS1 (veh. 44·6 mm ± 39·2) and the different treatment doses (FTY720 3.3 ng/µl, 542·3 mm ± 238·8; FTY720 1ng/µl, 615·3 mm ± 330·8; FTY720 0.3ng/µl, 670·3 mm ± 476·6). (C) Ceramides (Cer), dihydroceramides (DhCer), and the ratios DhCer/Cer in zebrafish MO-control and MO-DEGS1 treated with 1 ng/µl of FTY720 (n=4 (5 larvae per tube/condition) larvae/condition at 5 dpf $^{++}$). Data are represented as percentage of total ceramides and dihydroceramides. The results are from three independent experiments. (D) Intracellular ROS is partially normalized by FTY720 in patient fibroblasts^{++} (n=3) compared to controls (n=3). Data are shown as the means ± SD; * $p<0·05$; ** $p<0·01$; *** $p<0·001$ after one-way^{+} or two-way^{++} ANOVA test followed by Tukey's post hoc test.

Family	Family 1		Family 2	Family 3		Family 4	Family 5	
Mutations	c.395A>G: p.(His132Arg)		c.397C>T/752dupT: p.(Arg133Trp)/ (Leu251Phefs*10)	c.341_342delTT/764A>G p.(Leu114Profs*11)/(Asn255Ser)		c.604delT p.(Tyr202Thrfs*8)	c.764A>G p.(Asn255Ser)	
Ethnicity	Pakistani		European/Caucasian	European Caucasian		Moroccan	Moroccan	
Consanguinity	yes		no	no		no	yes	
Family members	2 affected siblings		5 unaffected siblings	2 affected siblings		3 unaffected siblings	2 affected siblings	
Patient number	**Patient 1**	**Patient 2**	**Patient 3**	**Patient 4**	**Patient 5**	**Patient 6**	**Patient 7**	**Patient 8**
Sex	M	M	F	F	M	F	M	M
Death (age)	no	yes (7y)	no	no	no	yes (4 y)	no	no
Age at last exam	6 y	7 y	9 y	9 y	6 y	4 y	13 y	9 y
Age of onset (months)	2	0.5	12	6	6	1	24	24
Term	34 WG	35 WG	38 WG	38 WG	39 WG	38 WG	39 WG	38 WG
Birth WT; HT; OFC	2710g; 47cm; 37cm	2400 g; 46 cm;35 cm	4025 g; na; na	3883 g; 55,9 cm; na	4054 g; na; na	3200 g; 48.3 cm; na	3.115g; 50 cm;35 cm	3.600 g; 49 cm; 35 cm
Motor acquisitions (age)	none	none	sit unassisted (6m) standing (9m)	hold head; sit with support	hold head; sit with support	none	walking without support short distance (2 y)	walking with support (2 y)
Motor developmental score (MDS)	0	0	2	1	1	0	4	3
language acquisitions(age)	none	none	simple sentences	few words (1y)	none	2 words associated	sentences (5y) , simple reading	sentences
Regression (age)	no	no	1 y	no	no	no	10 y	no
Neurological signs	ax/limb dys; sp	ax/limb dys; sp	limb dys;sp; dysarthria	limb dys; sp	limb dys; sp	ax dys	sp; dysmetria	sp; dysmetria; dysarthria
Eyes abnormalities	slow pendular ocular movements; optic atrophy	slow pendular ocular movements	anisocoria	Nystagmus and abnormal saccades. Mild optic atrophy	none	nystagmus(1m) then no fixation	none	none
Acquired microcephalia (SD)	no (-2)	yes (-3)	no (0)	no (0)	no (0)	no (0)	no (0)	no (0)
Failure to thrive (SD Weight; SD Height)	yes (-4 W, -4 H)	yes (-4 W, -4 H)	yes (-2 W; -4H)	yes (-4 W; -4 H)	yes (-4 W; -4 H)	na	no (+1 W; +1 H)	no (-1 W; -1 H)
Gastrostomia	yes (2 y; no gain)	yes (4 y; no gain)	Formula fed	yes (2y gain)	yes(4 y few gain)	no	no	no
Seizures (onset age)	none	none	Partial complex and clonic	clonic tonic severe (22m) status epilepticus. Stop Ketogenic diet (5y)	clonic tonic (2y). Stop ketogenic diet (2y)	myoclonic	none	partial complexes
Other signs	none	Died suddenly of unrecognized cause	Hip dysplasia	Premature pubarche Kyphosis and scoliosis	Kyphosis and scoliosis	none	none	none
Abnormal nerve conduction velocities (<35m/s)	yes (3y)	yes (6y)	no (8y)	na	na	na	na	no (8 y)
Long latencies of central conductions (>+2DS)	na	na	na	na	na	na	na	BAEP; SEP

Table 1. Clinical description of family 1 to 5 (BAEP: Brain stem auditory potentials; VEP: visuel evoked potentials; SEP: Somatosensory evoked potentials; W: weight; H: height; OFC: occipitofrontal circumference; dys: dystonia; sp: spasticity; y: year; m month; nl: normal; na: not available; motor development score (0: no acquisition; 1 hold the head; 2 sit position without support; 3 walk with support; 4 walk unaided)).

Family	Family 6	Family 7	Family 8			Family 9	Family 10		Family 11	Family 12	Family13
Mutations	c.337A>G p.(Asn113Asp)	c.337A>G p.(Asn113Asp)	c.320G>A p.(Trp107*)			c.565A>G /764A>G p.(Asn189Asp)/Asn255Ser)	c.852_855del p.(Tyr284*)		c.110T>C/878G>A p.(Met37Thr)/(Trp293*)	c.320G>A p.(Trp107*)	c.517C>T, p.(Arg173*)
Ethnicity	Algerian	Algerian	Egyptian			Indian	European Caucasian		Chinese	Egyptian	Iranian-Lor
Consanguinity	yes	yes	yes			yes (4th generation)	no		no	yes	yes
Family members	1 unaffected sibling	2 affected siblings died <14 y, 2 healthy siblings	3 affected siblings			1 unaffected sibling	2 affected siblings		1 unaffected sibling	no sibling	no sibling
Patient number	**Patient 9**	**Patient 10**	**Patient 11**	**Patient 12**	**Patient 13**	**Patient14**	**Patient 15**	**Patient 16**	**Patient 17**	**Patient18**	**Patient19**
Sex	F	M	F	M	M	M	M	M	F	F	M
Death (age)	no	no	yes (5 y)	yes (2.5 y)	no	no	no	no	no	no	no
Age at last exam	9 y	20 y	5 y	2.5 y	4 y	18 y	1 y	4 y	5 y	7.5 y	10y
Age of onset (months)	1	1	1	1	1	4	4	5	4	1	3
Term	37WG	40 WG	39 WG	38 WG	38 WG	39 WG	39 WG	40 WG	39 WG	38 WG	39 WG
Birth WT; HT; OFC	3280 g; 49 cm; 34cm	3700g; 50cm; 36 cm	3500g; 48cm; 34.5cm	3200g; 50cm; 35.5cm	3100g; 51cm; 35cm	3300 g; 55 cm. na	3401g; na; na	3515g; na; na	3300 g; na; na	2500g; 48cm; 34cm	2950g; 44cm; 34 cm
Motor acquisitions (age)	hold head; sit with support	hold head; sit with support	none	none	none	sit unassisted (5 m)	hold head; sit with support	hold head; sit with support	hold head	none	none
MDS	1	1	0	0	0	2	1	1	1	0	0
language acquisitions(age)	none	none	none	none	none	single words (2y)	none	none	none	none	none
Regression (age)	no	no	no	no	no	6m	no	no	no	no	no
Neurological signs	limb dys; sp	ax/limb dys; sp	limb dys; sp	limb dys; sp	limb dys; sp	choreoathetosis; sp	sp	sp	sp	sp	dys; sp
Eyes abnormalities	nystagmus (1m), 1 episode of tonic-upgaze like (8y), ERG nl	nystagmus (1m) ERG nl	nystagmus. (1m) ERG nl	nystagmus.(1m ERG nl	nystagmus(1 m) ERG nl	nystagmus (4m)	nystagmus (4m)	nystagmus (5m)	none	nystagmus (1m)	nystagmus
Acquired microcephalia (SD)	no (-2)	no (-2)	no (-2)	no (-2)	no (+1)	na	no (+1)	no (+1)	na	yes (-4.8)	yes (-4)
Failure to thrive (SD Weight; SD Height)	yes (-3,5 w; -4 H)	yes (-5 W; -5 H)	yes (-4 W; -4 H)	yes (-4W; -4H)	no (-2 W; -2H)	yes (-6 W; -6 H)	no (-1.W; 0 H)	no (-2 W; -1 H)	no (-1 W; +2 H)	yes (-3.5W; -6H)	yes (-4.5W; -3.5 H)
Gastrostomia	no	yes (18y)	Feeding diffculties	Feeding diffculties	Feeding diffculties	yes (1 y)	yes (1 y)	yes (2.5 y)	no	no	Feeding difficulties, Dysphagia
Seizures (onset age)	clonic tonic (8m) with status epilepticus	myoclonic (2 y)	partial and myoclonic (3y)	toic, atonic (8 m)	tonic (2.5y)	tonic clonic (5y)	none	tonic clonic	none	Febrile (4y).	none
Other signs	gingival hypertrophy , scoliosis & hip dislocation > 4.5 years of age.	gingival hypertrophy. Severe scoliosis and joint contractions	Hemorrhagic infarction at the age of 3, coma for 10 days, severe deterioration	Died suddenly of unrecognized cause	none	joints contractures	Skin hypopigmentation.	scoliosis. Skin hypopigmentation.	none	none	Kyphosis,Coarse face, Hirsutism, Bruxism
Abnormal nerve conduction velocities	no (1 y;) yes (2y)	yes (3y)	no (4y)	na	no	no (17y)	no (1y)	no (4y)	no (4y)	yes (6y)	na
Long latencies of central conductions	VEP; BAEP	VEP; BAEP	VEP	VEP	VEP	na	BAEP	na	na	na	na

Table 2. Clinical description of family 6 to 13 (BAEP: Brain stem auditory potentials; VEP: visuel evoked potentials; SEP: Somatosensory evoked potentials; W: weight; H: height; OFC: occipitofrontal circumference; dys: dystonia; sp: spasticity; y: year; m month; nl: normal; na: not available; motor development score (0: no acquisition; 1 hold the head; 2 sit position without support; 3 walk with support; 4 walk unaided)).

Patient number	Patient 1	Patient 2	Patient 3	Patient 4	Patient 5	Patient 6	Patient 7	Patient 8	Patient 9	Patient 10	Patient 11	Patient 12	Patient 13	Patient 14	Patient 15	Patient 16	Patient 17	Patient 18	Patient19
MRI (age of acquisition)	5m	6y	8 y	2y; 4 y	2 y	1 y	6 y	8 y	8m; 2.5 y; 6 y	2 y; 12 y	2 y; 3 y	1 y	10 m	17 y	11m	6m; 2.5 y; 4y	8m; 16m	6 y	10y
hypomyelination according to age on the last MRI																			
cerebellum	+	no	no	no	no	+	no	no	+	+	no	+	+	no	no	no	no	na	No
brainstem	no	no	no	no	no	no	no	no	+	no	no	+	no	no	no	no	no	na	No
cc	+	+	no	no	no	no	no	no	no	no	no	no	+	no	+/-	no	+	na	+/-
internal capsules	no	no	no	no	no	+	no	no	no	+	no	no	+	no	no	no	+	na	no
periventricular WM	no	+	+	+	+	+	+	+	+	+	+	+	+	+	+	+	+	na	+
deep WM	no	+	no	+	+/-	+	no	no	+	+	+	+	+	no	+	+	+	na	+
subcortical WM	no	+/-	no	no	no	no	no	no	no	no	no	+	no	no	no	no	+/-	na	no
myelin progression	na	na	na	yes	na	na	na	na	yes	yes	yes	na	na	na	na	yes	yes	na	na
Basal ganglia abnormalities	hyper T2 thalami	hypo T2 pallidi; atrophy hyper T2 thalami	no	atrophy hyper T2 thalami	atrophy hyper T2 thalami	no	no	no	atrophy hyper T2 thalami	atrophy hyper T2 thalami	no	no	no	atrophy hyper T2 thalami	hyper T2 dentate nucleus , hyper T2 thalami	mild atrophy hyper Flair thalami	atrophy hyper T2 thalami	na	hypo T2 pallidi; atrophy hyper T2 thalami
other	none	hypo T1 in the occipital deep WM/subcortical junction	none	none	none	none	enlargment WR spaces	enlargment WR spaces. spinal cord normal	none	Hypo T1 in the occipital deep WM/	occipital hemorragic infarction at 3	none	none	none	none	no	no	na	no
calcifications (CT scan)	no	yes (periventricular)	na	na	na	na	na	na	no	no	yes (cerebellum)	yes (cerebellum)	yes (cerebellum)	na	no	no	na	na	na
atrophy																			
cerebellum	no	++	no	no	no	no	no	no	+	++	+	+	no	+	no	+	no	na	++
ventricule dilatation	+	+	no	no	no	+	no	no	no	+	+	no	no	no	no	+	no	na	+
cortical	no	no	no	no	no	no	no	no	no	++ (frontal and sylvian fissures)	+	+ (sylvian fissures)	+ (sylvian fissures)	no	no	no	no	na	++ (frontal and sylvian fissures)
CC	no	++	no	+ (spleniu m)	+ (spleniu m)	+	no	no	+	++	+	+	+	+	+	+	+ (spleniu m)	na	++
MRS					na	na	na	na		na	na	na	na	na	na		na	na	na
NAA	nl	low	nl	low					low							low			
Choline	high	high	nl	high					nl							nl			
lactates	-	+	-	-					+/-							-			

Table 3. MRI description (WM: white matter; + present; WR: Wirchow Robin; y: year; m month; nl: normal; na: not available).